Reconstruction of Summer Barents Sea Circulation from Climatological Data

G. G. Panteleev[1*], D. A. Nechaev[2] and M. Ikeda[3]

[1]*International Arctic Research Center-Frontier Research System for Global Change*
University of Alaska Fairbanks, 930 Kouykuk Drive, P. O. Box 757335
Fairbanks AK 99775-7335 USA
[2]*University of Southern Mississippi, Stennis Space Center, Mississippi, USA*
[3]*Graduate School of Environmental Earth Science, Hokkaido University, Sapporo, Japan*

[Original manuscript received 21 December 2004; in revised form 8 August 2005]

ABSTRACT *An estimate of the summer Barents Sea circulation is constructed as a four-dimensional variational inverse of the monthly hydrographic and atmospheric climatologies. The reconstructed evolution of temperature, salinity, and velocity fields provides the best fit to climatological data and satisfies dynamical and kinematic constraints of a primitive equation ocean circulation model. The data-optimized Barents Sea state is in general agreement with the existing schemes of circulation in the region. The circulation is characterized by the 3.2 Sv inflow from the Norwegian Sea with the Norwegian Atlantic Current. Approximately 1.5 Sv of this inflow recirculates along the northern flank of Bear Island Trough, while the major branch of the current crosses the Barents Sea and outflows through Franz Josef Land—Novaya Zemliya and the Kara Gate straits with transports of 1.1 Sv and 0.6 Sv, respectively. The data assimilation reveals an eastward current between the Great and Central banks and cyclonic circulation in the region between Central Bank and Novaya Zemliya. These two circulation features have recently been confirmed in a number of publications. The reconstructed surface heat and salt fluxes are in qualitative and quantitative agreement with the known observational estimates. The posterior error analysis and sensitivity experiments provide additional arguments in support of the reliability of the data assimilation results.*

RÉSUMÉ *[Traduit par la rédaction] On construit une estimation de la circulation dans la mer de Barent en été comme une inverse variationnelle à quatre dimensions des climatologies hydrographique et atmosphérique mensuelles. L'évolution reconstruite des champs de température, de salinité et de vitesse fournit le meilleur ajustement des données climatologiques et respecte les contraintes dynamiques et cinématiques d'un modèle de circulation océanique à équations primitives. L'état de la mer de Barents optimisé en fonction des données s'accorde assez bien avec les schémas existants de la circulation dans la région. La circulation est caractérisée par le débit de 3,2 Sv entrant dans le courant atlantique norvégien à partir de la mer de Norvège. Environ 1,5 Sv de ce débit recircule le long du flanc nord de la fosse de l'île aux Ours (Bjornoya) pendant que la branche principale du courant traverse la mer de Barents et passe par le détroit de l'archipel François-Joseph – Novaya Zemliya et le détroit Kara Gate, avec des transports de 1,1 Sv et 0,6 Sv, respectivement. L'assimilation des données révèle un courant vers l'est entre les bancs Great et Central et une circulation cyclonique dans la région entre le banc Central et Novaya Zemliya. Ces deux caractéristiques de la circulation ont récemment été confirmées dans plusieurs publications. Les flux reconstruits de chaleur et de sel à la surface s'accordent, tant sur les plans qualitatif que quantitatif, avec les estimations connues fondées sur les observations. L'analyse des erreurs et les tests de sensibilité réalisés par la suite fournissent des arguments supplémentaires à l'appui de la fiabilité des résultats de l'assimilation des données.*

1 Introduction

The Barents Sea (BS) is an important pathway for the mass, heat and salt exchange between the Atlantic and Arctic oceans. The analysis of recent and historical data (Schauer et al., 2002) shows that the outflow rate from the BS and characteristics of the exported water masses play a crucial role in the formation of the water properties in the Arctic Ocean. The water outflowing from the BS is a result of the transformation of warm (3°–6°C) and saline (34.6–34.9 psu) Norwegian Atlantic water carried by the Norwegian Atlantic Current (Fig. 1) into the BS between Bear Island and the northernmost coast of Norway (Fig. 1). Part of this current returns to the Norwegian Sea along the northern slope of Bear Island Trough, while the major branch of the current crosses the BS and outflows through the opening between Franz Josef Land (FJL) and Novaya Zemliya (NZ) and through the Kara Gate strait. In fall and winter, strong atmospheric cooling in the BS causes significant modification of the Atlantic water properties as the water mass propagates to the east. According to Midttun (1985), winter cooling in the numerous banks and shallows adjacent to NZ forms saline and cold dense water, which subducts along the bottom slopes and then outflows through the opening between NZ and FJL. The export of dense water from the BS reaches maximum values during the winter but still remains significant in summer (July–September). In summer, the atmosphere warms the

*Corresponding author's e-mail: gleb@iarc.uaf.edu

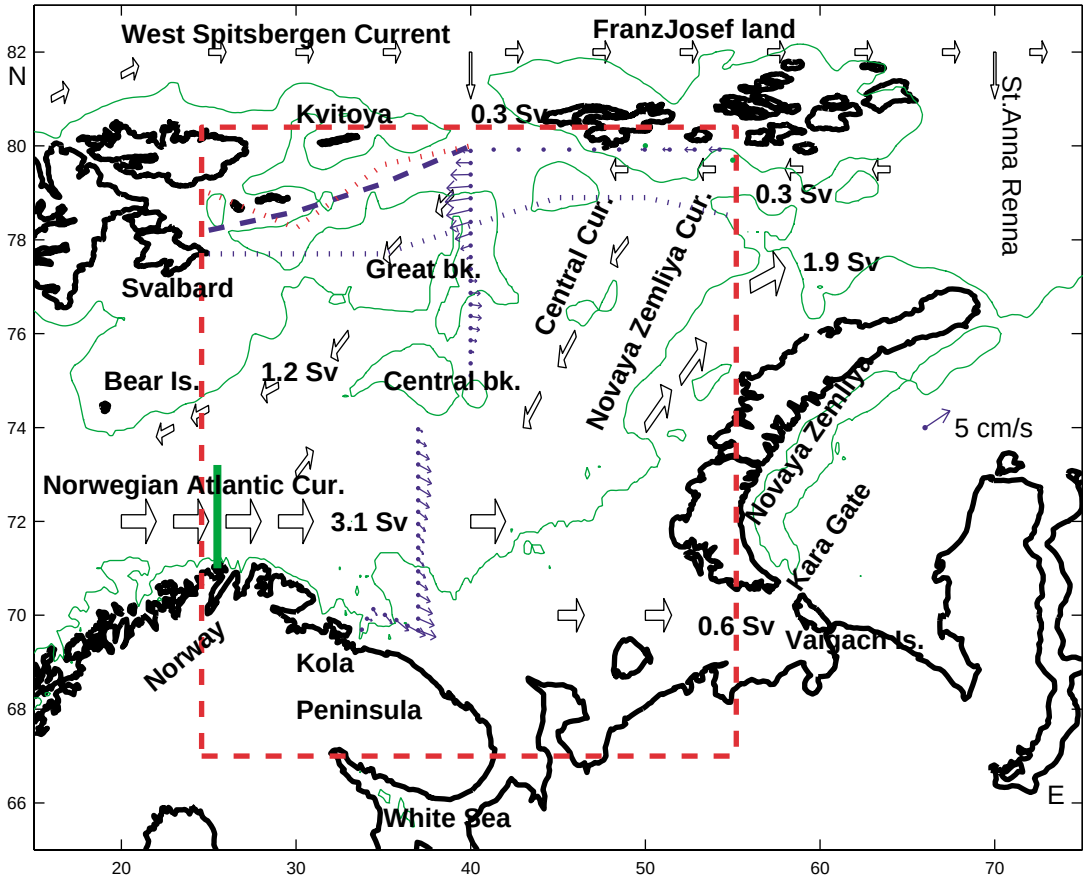

Fig. 1 Bottom topography in the BS. The thin line shows the 200-m isobath. The dashed line marks the boundary of the region investigated. The thick green line marks the section which was used for the comparison with the results of Ingvaldsen et al. (2002). Unfilled arrows show the scheme of major currents according to Tantsiura (1959). The estimates of corresponding mass transport are taken from Loeng et al. (1997). Solid blue arrows show the averaged velocities in the BS during the summer of 1997 at 60-m depth (Panteleev et al., 2004). The dotted blue, dashed blue and dotted red lines mark the averaged position of the ice edge in July, August and September, respectively.

surface layer at the rate of 50–200 W m^{-2} (da Silva et al., 1994; Makshtas and Ivanov, 1997), and causes gradual ice melting in the northern regions of the BS resulting in significant surface fresh water fluxes.

In the last decade a large volume of temperature, salinity and hydro-chemical data have been collected in the region (ACSYS, 1999; Matishov et al., 1998). These data provided a solid background for analysis of the origin and transformation of the water masses in the BS (Pfirman et al., 1994; Jones et al., 1998; Aagaard et al., 1985). Unfortunately, the water mass analysis provides only indirect estimates of the absolute velocities and mass transports, while the number of direct velocity measurements in the region is obviously insufficient. According to Loeng and Saetre (2001), in the last three decades there were about 70 mooring velocity measurements. Most of these moorings were located in the western part of the BS and only four of them were deployed in the FJL–NZ strait in 1991–92. These four moorings revealed a clear seasonal cycle in the outflow from the BS with transports of 2.5–3.1 Sv in winter and about 1 Sv in summer. At the same time, Panteleev et al. (2004) obtained an estimate of 0.1 Sv for the inflow into the BS between NZ and FJL in September 1997. The recent year-long velocity measurements (Ingvaldsen et al., 2002) did not show a clear seasonal cycle but revealed strong monthly variability in the throughflow between the northernmost coast of Norway and Bear Island with the amplitude of the transport variations up to ±5 Sv, while the estimate of the mean net inflow into the BS is about 2 Sv. High transport variability in the BS can be attributed to the barotropic nature of the BS circulation (Blindheim, 1989; Haugan, 1999) and the strong seasonal and interannual variability of the Norwegian Atlantic Current (Furevik, 2001; Mork and Blindheim, 2000; Ingvaldsen et al., 2004).

The sparseness of velocity measurements and the strong variability of the currents make quantitative estimates of the general circulation in the BS a difficult task. In this situation, hydrographic climatology, which is available for the whole basin, is a reliable source of information on the BS circulation. Unfortunately, attempts to recover the BS circulation from hydrographic data are usually based on algorithms, which suffer from a number of problems. The dynamical

method for the calculation of geostrophic currents (Helland-Hansen, 1934) cannot recover absolute velocity unless a reference velocity is prescribed at some level in the ocean (Tantsiura, 1959; Uralov, 1960; Potanin and Korotkov, 1988), while application of sophisticated numerical models requires specification of the model boundary conditions and forcing, which are subjected to significant uncertainties (Harms, 1997; Yakovlev, 1999; Trofimov, 2000). These errors and uncertainties may explain the discrepancies between the results of various numerical simulations. For example, Yakovlev (1999) utilized open boundary conditions extracted from the Arctic Ocean circulation model which revealed a 0.3 Sv outflow between Svalbard and FJL, while Trofimov (2000) diagnosed a 0.4 Sv inflow into the BS.

In this paper, we utilize a method which closes the gap between the circulation estimates which rely heavily on observations (such as the dynamical method and water mass analysis), and the estimates based on dynamical constraints alone (such as model simulations). Our goal can be formulated as follows: we are looking for the BS circulation which is capable of reproducing the evolution of the hydrographic fields documented in climatological atlases, and which satisfies the dynamical constraints of a primitive equation model (Nechaev and Panteleev, 2000). To reproduce the evolution climatological data we tune the initial and boundary conditions of the model using a four-dimensional variational data assimilation (4D-var) technique (Le Dimet and Talagrand, 1986). The reliability of the reconstructed circulation is tested through the statistical analysis of the posterior errors: we generate a simulated ensemble of datasets and estimate the sensitivity of the data assimilation results with respect to data errors and uncertainties in the specification of the data assimilation parameters.

The approach described in this paper has been successfully implemented in a number of studies (e.g., Grotov et al., 1998; Nechaev et al., 2004). The method allows us to overcome the reference velocity problem of the dynamical method and to minimize the effects of poorly known open boundary conditions and surface forcing. The region under investigation is shown in Fig. 1. The model domain covers the major water transformation regions in the BS, though it is slightly smaller than the conventional boundaries of the BS. The western boundary of the model domain was chosen east of Bear Island to avoid consideration of deeper areas and to reduce the computational cost of the data assimilation.

The paper is organized as follows. We start with the description of available data and their preliminary analysis (Section 2). The outline of the numerical model utilized, statistical hypotheses and specific details of the variational data assimilation procedure are discussed in Section 3. In Section 4 we present the major results of the reconstruction of the summer BS circulation and provide an error analysis of the data assimilation results. Discussion and conclusions are provided in Section 5.

2 Data

The reconstruction of the summer circulation in the BS is based on the following datasets: i) the climatological distributions of temperature and salinity from the BarKode hydrophysical atlas produced by ACSYS (1999); ii) the monthly mean surface drifter velocities collected in the region in 1991–95 (Poulain et al., 1996); iii) monthly wind stress climatology (da Silva et al., 1994); and iv) estimates of total transports through the segments of the open boundary taken from the literature. Data assimilation prescribes relative weights to different data according to the reliability of the observations. Therefore the analysis of the datasets in this section includes the specification of the prior data error variance. Variance of the data errors takes into account both instrumental and interpolation errors. The signals of processes which are not described by the model (e.g., interannual variability of the observations and data variability on weekly timescales) are also treated as data errors.

a *Hydrography*

Approximately 80,000 temperature and salinity profiles for July, August and September were extracted from the BarKode hydrophysical atlas (ACSYS, 1999) (the total number of profiles is 206,300). The assimilation of raw temperature/salinity profiles into the model is not computationally efficient since, in many cases, the individual profiles do not represent statistically independent climatological observations under the constraints of the model dynamics. Therefore the temperature/salinity data were first interpolated onto the model grid.

The model grid is a regular z-coordinate grid with a meridional resolution of 0.2° and a zonal resolution of 0.6°. Vertically, the grid has 17 levels with unequal spacing ranging from 7.5 m at the surface to 50 m at the deeper levels. The horizontal interpolation of temperature and salinity was performed by the algorithm, which has previously been used for the compilation of the BS region hydrographic atlas (Golubev et al., 1992; Matishov et al., 1998). The algorithm calculates the interpolated value as a weighted sum of the temperature/salinity data within the "radius of influence", R, with the weights being the functions of the distance between the interpolated point and the data location. According to Denisov et al. (1987), this interpolation algorithm avoids oversmoothing of the interpolated fields in the straits and near the coast.

The standard deviation, σ_C, of the gridded temperature and salinity was estimated as

$$\sigma_C = \left[1/(N-1)\sum_n^{r<R}\left(C_n - \overline{C_{R,N}}\right)^2\right]^{\frac{1}{2}}, \quad N > 3$$
$$\sigma_C = (2°\mathrm{C}, 0.2\ \mathrm{psu}), \quad N \le 3,$$

where C stands for the temperature and salinity fields, $C = (T,S)$, $\overline{C_{R,N}}$ is the average of C within a circle of radius R, and N is the number of measurements within the circle. The radius R, with typical values of R = 100 km, is equal to the radius of influence used in the data interpolation.

The gridded temperature and salinity data at 30-m and temperature data at 200-m depth for July–September are shown in Fig. 2 and Fig. 3. An example of the spatial distribution of

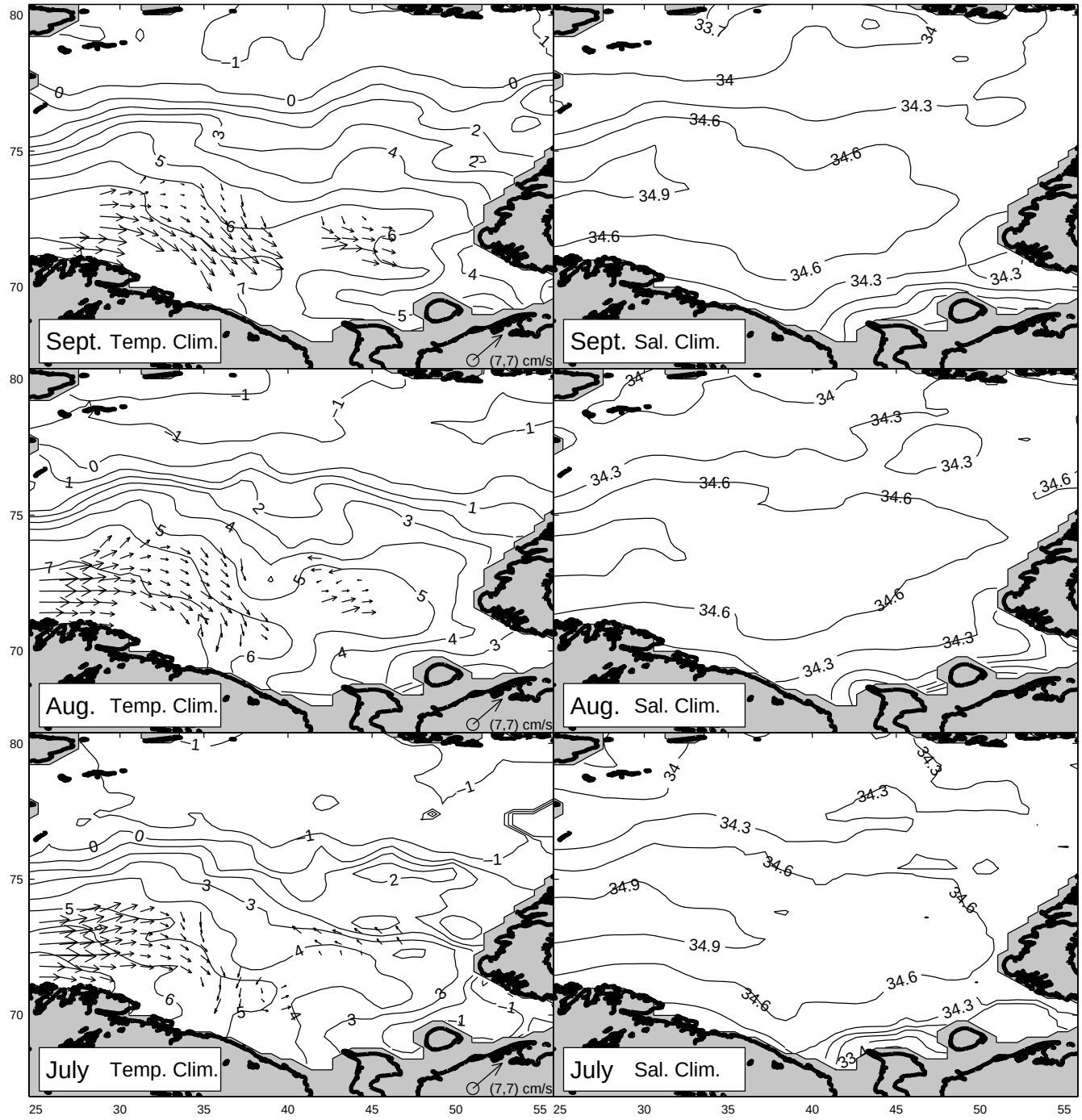

Fig. 2 Summer climatological temperature (left panels, °C) and salinity (right panels, psu) distributions at 30-m depth. Arrows show the currents calculated from surface drifters (Poulain et al., 1996).

temperature standard deviation, σ_T, is presented in the left panels of Fig. 3. Higher values of σ_T in the central part of the BS indicate stronger natural variability in this region. The spatial irregularity of σ_T in the northern part of the region is a consequence of data sparseness due to the rough ice conditions (Fig. 1). The spatial distribution of salinity, σ_S, exhibits similar features.

b *Drifter Velocities*

Monthly mean surface currents were estimated from a set of surface drifter trajectories collected from 1991–95 in the Norwegian Sea and the BS (Poulain et al., 1996). Since there were a limited number of drifters in the BS, temporal and spatial averaging was performed to obtain statistically reliable estimates for the surface currents. One-year long records of

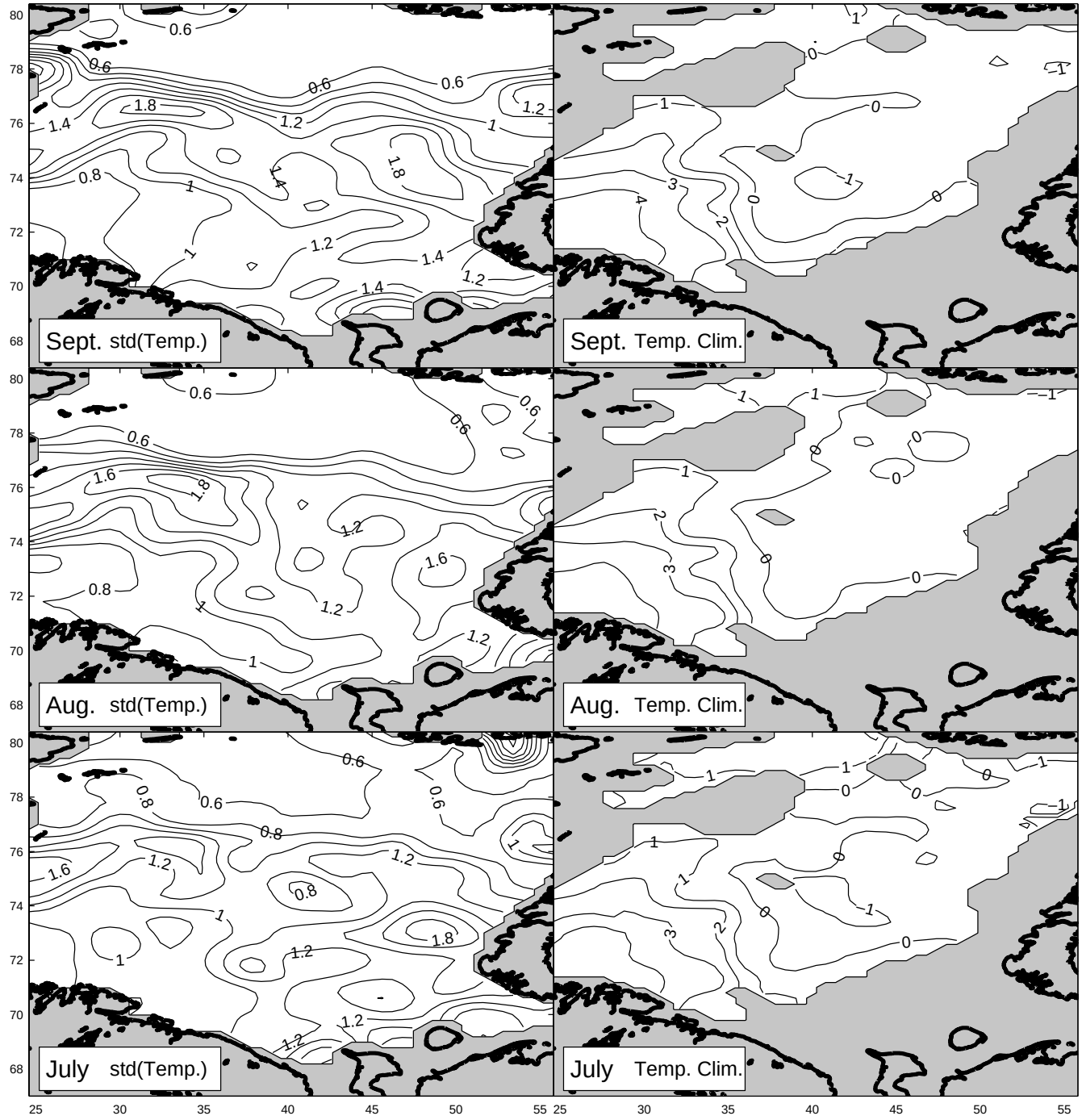

Fig. 3 Estimates of σ_T of climatological temperature at 30-m depth (left panels, °C) and summer climatological temperature distribution at 200-m depth (right panels, °C).

current meter moorings between Bear Island and the Norwegian coast (Ingvaldsen et al., 2002) revealed that the characteristic spatial scales of local currents vary between 50 km and 150 km. Adopting these typical scales for the south-eastern BS we interpolated drifter velocities (where available) onto the model grid by using following the temporal and spatial averaging procedure:

$$\mathbf{u}^*(x_0, y_0, t_0) = \sum w_i \mathbf{u}(x_i, y_i, t_i) / \sum w_i,$$

$$w_i = \exp\left(-(t_i - t_0)^2 / t_u^2\right) \exp\left(-r_i^2 / R_u^2\right),$$

where $\mathbf{u}$ (x_i, y_i, t_i) denotes drifter velocity at the point (x_i, y_i, t_i) obtained through finite difference differentiation along the

drifter trajectory with d_t = 1 day, t_u = 17 days, R_u = 80 km, x_0, y_0 are the coordinates of the grid node, t_0 is the fifteenth day of each summer month, $r_i^2 = (x_i - x_0)^2 + (y_i - y_0)^2$, and the summation is done over all drifters and all grid nodes in the area where the drifters are available. The standard deviation of the interpolated surface velocities was estimated as

$$\sigma_{\mathbf{u}^*} = |\mathbf{u}^*| / \left(N_d - 1\right)^{0.5} + 1 \text{ cm s}^{-1},$$

where N_d is the number of statistically independent estimates of the velocity derived from drifter tracks. For the surface velocity data, which have been accepted for data assimilation, this number varied between 2 and 6, which gives an estimate for $\sigma_{\mathbf{u}^*}$ of approximately 30–50% of the local velocity amplitude.

The estimated surface velocities for July–September are shown in Fig. 2. Most of the surface drifters (Poulain et al., 1996) were observed in the western part of the BS, therefore, the estimates of the surface velocity are more reliable in the region between 25°E and 30°E, and the reliability of drifter velocity gradually decreases to the east. Drifter velocities located east from 40°E were ignored as statistically unreliable. The estimates of surface velocities obtained cover only a small part of the BS but they provide valuable information on the inflow conditions and the Norwegian Atlantic current.

A limited number of current measurements were collected in the BS by Norwegian scientists (Loeng and Saetre, 2001). We did not assimilate these data but used them for validation of data assimilation results.

c *Volume Transports*

The circulation in the BS is predominantly barotropic (Haugan, 1999), therefore the estimates of the transports through the different sections of the open boundary are very important for the reconstruction of the circulation. Historically, the first estimates of the transport in the BS were based on the calculation of geostrophic currents (Uralov, 1960; Potanin and Korotkov, 1988). Direct velocity measurements collected from 1960–97 allowed Loeng et al. (1997) to formulate a general scheme of the annual mean volume budget of the BS shown in Fig. 1.

Almost all investigators (e.g., Uralov, 1960; Potanin and Korotkov, 1988; Loeng et al., 1993) reported the presence of a clear seasonal cycle in the BS circulation. Therefore, the available estimates of the annual mean volume transport (Loeng et al., 1997) cannot be used directly for the reconstruction of the summer circulation and require some corrections to take into account seasonal variability. In this section, we present a brief analysis of the available transport estimates through the BS openings during the summer period.

According to Uralov (1960) and Potanin and Korotkov (1988), the water exchange between the BS and the White Sea is almost negligible (0.01 Sv) and equal to the fresh water discharge into the White Sea. The river discharge is usually well documented, therefore these estimates seem to be quite reliable.

Most of the transport estimates through the Kara Gate (Uralov, 1960; Potanin and Korotkov, 1988; Scherbinin, 2001) have a net outflow of 0.6–0.7 Sv. These estimates are based on both geostrophic calculations (Uralov, 1960) and direct velocity measurements (Scherbinin, 2001; Panteleev et al., 2004). In the current study we adopted the value of 0.65 ±0.2 Sv as the Kara Gate transport estimate.

The estimates of the net transport between FJL and NZ are rather controversial. The geostrophic calculations (Uralov, 1960; Timofeev, 1963) indicate a 0.2–0.5 Sv outflow from the BS, while the year-long velocity measurements (Loeng et al., 1993) reveal seasonal transport variations, with a net outflow approximately 0.8–0.9 Sv in summer and approximately 2.4 Sv in winter. The estimates of the transport made by Loeng et al. (1997), were based on the records from four moorings (the fifth mooring, which was the most northerly, was lost during the experiment) and did not take into account transports in the northern part of the strait. The presence of a westward current along the southern flank of FJL, which is documented in Tantsiura (1959), may result in a slight overestimation of the net outflow through the FJL–NZ strait in Loeng et al. (1997). Therefore, for the data assimilation we used the transport estimates of Loeng et al. (1993) (0.8 Sv and 1.6 Sv for the transports in June and October respectively), and prescribed an outflow of 1 ±0.3 Sv as the summer transport through the FJL–NZ strait.

The transport between Spitsbergen and FJL has not been well studied. The analysis of water masses by Pfirman et al. (1994), and the study of the summer 1996 hydrographic data by Loyning (2000) both indicate inflow into the BS from the Arctic Ocean. In the absence of other estimates we follow the mass balance scheme of Loeng et al. (1997) and prescribe 0.4 ±0.2 Sv as a first guess for this inflow.

The velocity measurements in the western part of the BS from September–October 1978 (Blindheim, 1989) reveal an inflow of 3.1 Sv between Norway and 73°N latitude, and an outflow of 1.2 Sv along the southern flank of Bear Island. Ingvaldsen et al. (2002) present similar estimates for the summer transport but reported a strong monthly variability in the net transport between Norway and Bear Island with a standard deviation of 2 Sv. Both of these estimates are based on the velocity measurements along the southern part of the western boundary of the BS (south of 73.5°N), and cannot be treated as a net transport through the western opening of the BS. Therefore, in this study we derive the net transport estimate through the western open boundary of the model region using the condition of conservation of volume. The estimates of the inflow between 73°N and the Norway coast (Blindheim, 1989; Ingvaldsen et al., 2002) are used as independent data for cross-validation of assimilation results.

The estimates of the transports through different segments of the open boundary of the BS are summarized in the left and centre columns of Table 1. We incorporate a gradual increase in the transport through the western boundary and the FJL–NZ strait from July–September in agreement with the studies of Uralov (1960), Potanin and Korotkov (1988), and Loeng et al. (1993) which indicate an intensification of the BS circulation in October–November.

TABLE 1. Transports through the open boundaries of the BS (estimates taken from literature, first guess, and optimized).

Boundary part	Transport (Sv) from literature	First guess transport (Sv)			Optimized transport (Sv)		
		July	August	September	July	August	September
western	1.2 – 2.1	1.14 ± 0.3	1.24 ± 0.3	1.34 ± 0.3	1.23	1.38	1.44
southern	0.007	0.01 ± .005	0.01 ± .005	0.01 ± 0.005	0.02	0.02	0.02
Kara Gate	0.6 – 0.7	–0.65 ± .2	–0.65 ± .2	–0.65 ± 0.2	–0.65	–0.65	–0.69
FJL–NZ	0.0 – 1.35	–0.9 ± 0.3	–1.00 ± 0.3	–1.1 ± 0.3	–1.0	–1.1	–1.17
northern	0.3	0.4 ± 0.2	0.4 ± 0.2	0.4 ± 0.2	0.4	0.35	0.4

d *Meteorological Data*

The half-by-half degree gridded wind stresses were extracted from the monthly climatology of da Silva et al. (1994) and were linearly interpolated onto the model grid. The resulting wind stress fields are rather smooth with the characteristic spatial scales of the order of the basin size. To allow for the adjustment of the spatial details in the model forcing we used wind stress data with a relatively high error variance, equal to 40% of the wind stress spatial variability in the BS.

According to da Silva et al. (1994), surface heat fluxes in the BS are approximately 100 W m^{-2}, 30 W m^{-2} and –50 W m^{-2} in July, August, and September respectively. Summer mean surface salt fluxes vary from 1.0×10^{-7} kg m^{-2} s^{-1} to -4.0×10^{-7} kg m^{-2} s^{-1}. The spatial structure of the da Silva et al. (1994) climatological fluxes is extremely smooth and does not reflect ice melting in the northern regions. At the same time, realistic surface heat and salt fluxes depend strongly on the state of the oceanic mixed layer and may exhibit high spatial and temporal variability. Because of that, the surface heat and salt climatologies of da Silva et al. (1994) were not used as "flux data" in the assimilation procedure. Instead, the surface flux climatologies were compared with the reconstructed fluxes for the validation of the data assimilation results. In such a comparison we treat the da Silva et al. (1994) climatologies as independent data even though the typical values for heat/salt fluxes and the corresponding spatial scales were used for the calculation of the smoothness term weights in the cost function outlined in Section 3b.

3 Data assimilation technique

a *Forward and Adjoint Models*

To derive the BS circulation from the data, the observational information should be combined with the information imposed by dynamical constraints. The dynamical constraints are formulated as a numerical model based on the set of conventional primitive equations under Boussinesq and hydrostatic approximations. The model can be viewed as a modification of the C-grid, *z*-coordinate Ocean General Circulation Model (OGCM) designed at the Laboratoire d'Oceanographie Dynamique et de Climatologie (Madec et al., 1999). The model is implicit both for barotropic and baroclinic modes permitting model runs with relatively large time steps. The model is used in "climatological" non-eddy-resolving mode on a relatively coarse grid with a six-hour time step. The model is also subjected to a number of simplifications, which do not compromise the validity of the major dynamical balances of the BS circulation. First of all, we do not utilize any ice model. This is acceptable because most of the basin is ice free in summer. On the other hand, surface fluxes, which can be modified by the presence of ice, are free parameters of the model to be tuned in data assimilation. So the surface fluxes obtained in data assimilation experiments can be interpreted as the fluxes at the ice-water interface, but not necessarily as the atmospheric fluxes.

The second simplification is related to the turbulence closure. The mixing processes in the model are parametrized by the prescribed vertical and horizontal eddy diffusion coefficients and the hydrostatic adjustment algorithm. The non-uniform and non-stationary temperature and salinity vertical diffusivity coefficients for data assimilation experiments were obtained as an average over the ensemble of the forward runs of the model using Pacanowski and Philander's (1981) turbulence closure. After that, these coefficients were smoothed in time and space and used as fixed parameters in the experiments outlined below. The values of the coefficients ranged between 5×10^{-4} m^2 s^{-1} at the surface and 2×10^{-5} m^2 s^{-1} near the bottom. The vertical momentum diffusivity coefficient was constant at 5×10^{-5} m^2 s^{-1}. Horizontal momentum and temperature and salinity diffusivity coefficients were to set 10 m^2 s^{-1}. In the data assimilation experiments we obtained an indication that this simplification might not be accurate in the shallow regions near the coast of Russia resulting in larger model data misfits. But we had to use this sub-optimal parametrization of the mixing processes since the adjoint code for more advanced turbulence closures is not yet available.

The adjoint code of the model was built analytically by transposition of the operator of the tangent linear model, linearized in the vicinity of the given solution of the forward model (Penenko, 1981; Wunsch, 1996). Application of the implicit scheme with large time steps results in a considerable reduction in storage requirements for variational data assimilation since, for non-linear problems, running the adjoint model requires storing the solution of the forward model at every time step. The tangent linear model was obtained by direct differentiation of the forward model code. Therefore, the tangent linear and adjoint models were the exact analytical consequences of the forward model. An illustration of the method for the construction of the adjoint procedure for the hydrostatic adjustment algorithm is presented in Appendix A.

In the course of data assimilation, the model solution is optimized by tuning free parameters (the so-called control vector) of

the model. The control vector of the model is composed of values of the functions specifying initial conditions, open boundary conditions and surface fluxes. The set of initial conditions of the model includes sea surface height (SSH) fields, temperature, salinity and horizontal components of velocity. Boundary components of the control vector are comprised of the distributions of temperature, salinity, and normal components of velocity specified on the open boundaries. The free-slip boundary condition for the tangent velocity component is set on the open boundary, therefore the values of the tangent velocity are not included in the control vector.

b *Cost Function*

The variational data assimilation can be formulated as a traditional least squares problem (Marchuk, 1974; Penenko, 1981; Le Dimet and Talagrand; 1986, Thacker and Long, 1988). The optimal solution of the model is found through constrained minimization of a quadratic cost function on the space of the model control vectors, where the cost function measures squared weighted distances between the model solution and data.

Statistical interpretation of the least squares method (Thacker, 1989; Wunsch, 1996) considers the cost function as an argument of the Gaussian probability distribution with the cost function weights being the inverse covariances of the corresponding data errors. Under the statistical interpretation the optimal solution is the most probable model state for the given data realization and prior error statistics.

Because of the sparseness of the oceanographic data and limited duration of observational time series, practical data assimilation methods commonly rely on the assumption that the errors of different observations are δ-correlated (Thacker, 1989). Under this assumption the cost function weights are represented by the diagonal matrices, with diagonal elements being equal to the reciprocals of the corresponding data error variances.

In the present study we use the cost function $\mathcal{J}$, which, in addition to the "real" climatological data described in Section 2, contains the so-called "bogus" data (Thacker, 1989) in the form of the smoothness terms:

$$\mathcal{J} = \mathcal{J}_C + \mathcal{J}_{\mathbf{u}}$$

$$\mathcal{J}_C = \int_{\Omega,t}\left[W_C^{-1}(C - C^*)^2 + W_C^{s-1}(\Delta C)^2\right]d\omega dt + \int_{z=0}\left[W_B^{s-1}(\Delta B)^2\right]dsdt$$

$$\mathcal{J}_{\mathbf{u}} = \sum_K W_{\mathbf{u}_k}^{-1}\left(\mathbf{u} - \mathbf{u}_k^*\right)^2 + \sum_{n=1,N} W_{V,n}^{-1}\left(\int_{-H}^{0}\mathbf{u}dz - V_n^*\right)^2 + \int_{\Omega} W_{\mathbf{u}}^{s-1}(\Delta\mathbf{u})^2\,d\omega dt + \int_{z=0}\left[W_\zeta^{s-1}(\Delta\zeta)^2 + W_{\boldsymbol{\tau}}^{-1}(\boldsymbol{\tau} - \boldsymbol{\tau}^*)^2 + W_{\boldsymbol{\tau}}^{s-1}(\Delta\boldsymbol{\tau})^2\right]dsdt.$$

Here $\mathbf{u}$ denotes the horizontal velocity; ζ is the sea surface height ; $C = (T,S)$ where T is temperature and S is salinity; $\boldsymbol{\tau}$ is the wind stress; B denotes the surface heat and salt fluxes; K is the number of velocity data points derived from surface drifters; N is the number of segments of the open boundary; V_n is the estimate of transport through the nth segment of the open boundary, $W_{\cdots}^{\cdots}$ denotes the variances of the corresponding data. Asterisks denote the observed fields. The smoothness or "bogus" data terms in $\mathcal{J}$ are proportional to the squared Laplacians of the model fields. These terms were introduced into the cost function to regularize the data assimilation problem. Bogus data terms remove high frequency noise from temperature fields in the north-eastern part of the BS and compensate for the lack of velocity data.

The cost function, $\mathcal{J}$, contains two groups of terms, $\mathcal{J}_C$ and $\mathcal{J}_{\mathbf{u}}$, which constrain baroclinic (temperature, salinity and heat/salt fluxes at the surface) and barotropic (SSH, velocity and wind stress) variables of the model respectively. The physical meaning of different terms in $\mathcal{J}_C$ and $\mathcal{J}_{\mathbf{u}}$ is straightforward: minimization of these terms enforces smoothness of the model solution and makes it tend to the observed data.

The spatial and temporal distributions of "real" data variances $W_{\cdots}^{\cdots}$ were discussed in the Section 2. The variances of the "bogus" data, W_C^s, W_B^s, $W_{\mathbf{u}}^s$, W_ζ^s, $W_{\boldsymbol{\tau}}^s$ are determined through the scale analysis: $W_C^s = L_C^4/C_s^2$, $W_B^s = L_C^4/B_s^2$ $W_{\mathbf{u}}^s = L_{\mathbf{u}}^4/V_s^2$, $W_\zeta^s = L_{\mathbf{u}}^4/\zeta_s^2$, $W_{\boldsymbol{\tau}}^s = L_{\boldsymbol{\tau}}^4/\boldsymbol{\tau}_s^2$. The scales $V_s = 5$ cm s^{-1}, $\zeta_s = 10$ cm are defined as typical variations of these variables in the first guess solution (Fig. 4), while the parameters C_s^2, B_s^2, $\boldsymbol{\tau}_s^2$ are derived from characteristic spatial variability of the corresponding data. We utilized a uniform spatial scale for the wind stress fields $L_{\boldsymbol{\tau}} = 500$ km, while spatial scales L_C and $L_{\mathbf{u}}$ were the functions of the local depth gradient and varied within the ranges 100–300 km and 50–150 km respectively. This setting of the characteristic scales allows us to avoid over smoothing of the model solution in the regions with strong topographic steering.

The mathematical aspects of the constrained minimization of $\mathcal{J}$ are outlined in a number of papers (e.g., Marchuk, 1974; Thacker, 1989; Penenko, 1981; Wunsch, 1996). We utilize a standard iterative method for cost function minimization. Starting with some prior estimate of the model control vector we perform the model run to obtain the so-called first guess solution. Given the solution of the forward model we compute the value of the cost function $\mathcal{J}$ and run the adjoint model backwards in time to estimate the gradient of the cost function with respect to the control vector. The gradient of the cost function is then used in the quasi-Newtonian optimization algorithm (Gilbert and Lemarechal, 1989) to find a better estimate of the control vector of the model. The procedure is repeated until the norm of the cost function gradient is sufficiently small.

Because of the model non-linearity, the cost function, $\mathcal{J}$, may have multiple local minima. The quasi-Newtonian optimization algorithm finds only one local minimum, which is the closest to the first guess solution. Therefore, the proper choice of the first guess solution is important. To prepare the first guess solution,

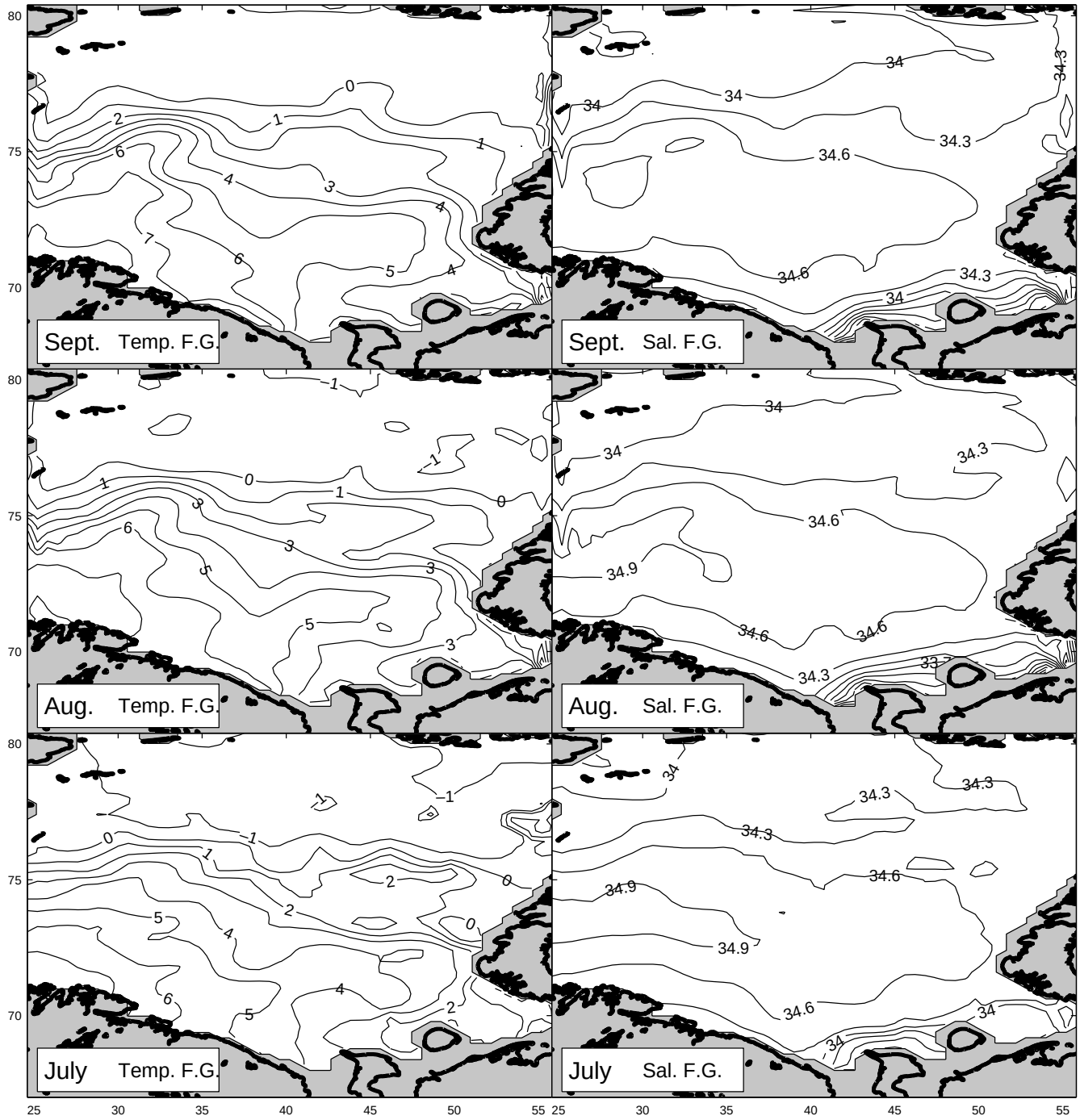

Fig. 4 First guess solution. Evolution of temperature field (°C) at 30-m depth.

which is reasonably close to the observed data, the calculation of the the first guess solution was performed in two steps. First, we solved 3D-var data assimilation problems to find the optimal steady state diagnostic velocity fields for July, August and September respectively. At this stage we are looking for the open boundary velocities, which minimize the cost function:

$$\mathcal{J}^1_{\mathbf{u}} = \sum_K W^{-1}_{\mathbf{u},k}\left(\mathbf{u} - \mathbf{u}^*_k\right)^2 + \sum_N W^{-1}_{V,n}\left(\int_{-H}^{0} \mathbf{u}dz - V^*_n\right)^2 + \int_\Omega W^{s-1}_{\mathbf{u}}(\Delta\mathbf{u})^2\, d\Omega + \int_{z=0} W^{s-1}_{\zeta}(\Delta\zeta)^2\, dS,$$

separately for the July, August and September data under the dynamical constraints of the steady state diagnostic model. The cost function weights for 3D-var data assimilation are the same as for the full 4D-var problem. The cost function, Eq. (2), is minimized under the constraints of the steady state momentum and continuity equations. The advection terms are ignored in the momentum equation. The solution of the steady state model is optimized by tuning the normal velocity distribution on open boundaries. Temperature and salinity distributions and wind stress fields are kept fixed. The mathematical meaning of this approach is straightforward: the solution of the minimization problem should provide an optimal set of open boundary conditions which gives physically reasonable velocity and SSH fields in the interior of the model domain.

On the second step, we run the full model for the period between 15 July and 15 September. The model run starts from the velocity and SSH fields obtained diagnostically for July, while the initial distributions for temperature and salinity are taken from the corresponding climatological data (Fig. 2). The values of the fields on the open boundary and the surface fluxes are obtained by linear interpolation of the diagnosed states in time.

Figure 4 shows the evolution of the temperature field in the first guess solution at a depth of 30 m for the summer months. Inconsistencies between partly optimized velocity and non-optimized temperature and salinity on the open boundaries result in the formation of the artificial boundary layer along the western boundary. Comparison of the first guess solution with climatological data (Fig. 2a) reveals that the first guess solution gradually drifts away from the data.

Starting from the first guess solution (Fig. 4) we performed a minimization of the cost function, Eq. (1), for the entire set of data. To reduce the dimension of the control vector, the boundary conditions and surface fluxes were controlled once every six days with linear interpolation applied between the control time steps. The dimension of the control vector was approximately 250000 elements. Minimization of the cost function required about 300–500 iterations of the quasi-Newtonian optimization algorithm (Gilbert and Lemarechal, 1989) to reduce the gradient norm by 2–3 orders of magnitude.

4 Data assimilation results

a *Barents Sea Circulation*

Optimized transports through the open boundaries of the BS are presented in the third column of Table 1. The 0.02-Sv inflow through the southern boundary overestimates the first guess transport of 0.01 Sv (the second column of Table 1), while the averaged transports through other boundaries lie within the error bars of prior transport estimates. Optimized transports gradually increase from July to September in agreement with the prior transport estimates.

The optimized transport between 73°N and the Norway coast (marked by the green dotted line in Fig. 1) is equal to 2.9, 3.1, and 3.6 Sv for July, August and September respectively. These values are in good agreement with the mean summer inflow of 3.1 Sv obtained by Ingvaldsen et al. (2002). As mentioned above, in a data assimilation experiment we utilize only the transport estimates through the entire western boundary of our region, therefore the transport observations of Ingvaldsen et al. (2002) can be treated as independent data supporting our results.

The evolution of the optimized fields of temperature and salinity at 30 m is shown in Fig. 5. The comparison between climatological data (Fig. 2), first guess solution (Fig. 4) and optimized temperature fields (Fig. 5) reveals that data assimilation strongly improves agreement between the modelled and observed fields. Significant improvement of the modelled temperature can be seen in the western and southern parts of the BS, where optimization has removed an artificial boundary layer and attracted the modelled temperature to the "two-tongue" distribution in the data (see the upper panels in Figs 2, 5 and 6). Assimilation regularized the model solution in July, when the temperature and salinity data are obviously noisy in the north-eastern part of the BS (Fig. 2), and kept a similar level of smoothness in August and September when the spatial data coverage was more uniform. Selective filtration of the data noise in the reconstructed fields is the consequence of correct specification of the smoothness terms incorporated into the cost function, Eq. (1).

Figure 6 shows normalized differences between the first guess temperature, T_{fg}, and data, and the optimized temperature, T_{opt}, and data, estimated as

$$\varepsilon(z) = \left[\int_S \left(T - T^*\right)^2 ds \,/\, \int_S \left(T^* - \overline{T^*}\right)^2 ds \right]^{\frac{1}{2}}$$

for each level. Here, $\overline{T}^*$ is the mean climatological temperature at level z, $T = (T_{fg}, T_{opt})$. As was discussed in Section 4a, the optimized solution is much closer to the climatological data in August and September. Even more important is that the difference between optimized and climatological fields is uniform in time, while the first guess solution gradually departs from data. The relative errors, $\varepsilon(z)$, increase slightly with depth due to a significant decrease in the temperature variability in the lower layers, but the absolute errors remain smaller than the prior error estimates for the climatological data.

The regions with the worst visual agreement between climatological data and optimized temperature fields (Fig. 2 and Fig. 5) are located in the shallow regions of the south-eastern BS. There can be two reasons for this. Firstly, the climatological temperature (Fig. 3, left panels) and salinity (not shown) exhibit relatively high natural variability in these regions resulting in higher prior data error variances and lower cost function weights. Secondly, the vertical mixing in our model is defined by fixed coefficients, therefore the model cannot describe complicated mixing processes in the shallow regions. Note that in shallow regions the level of the 30-m depth is within the layer of the summer thermocline with a strong vertical gradient, therefore the model deficiencies

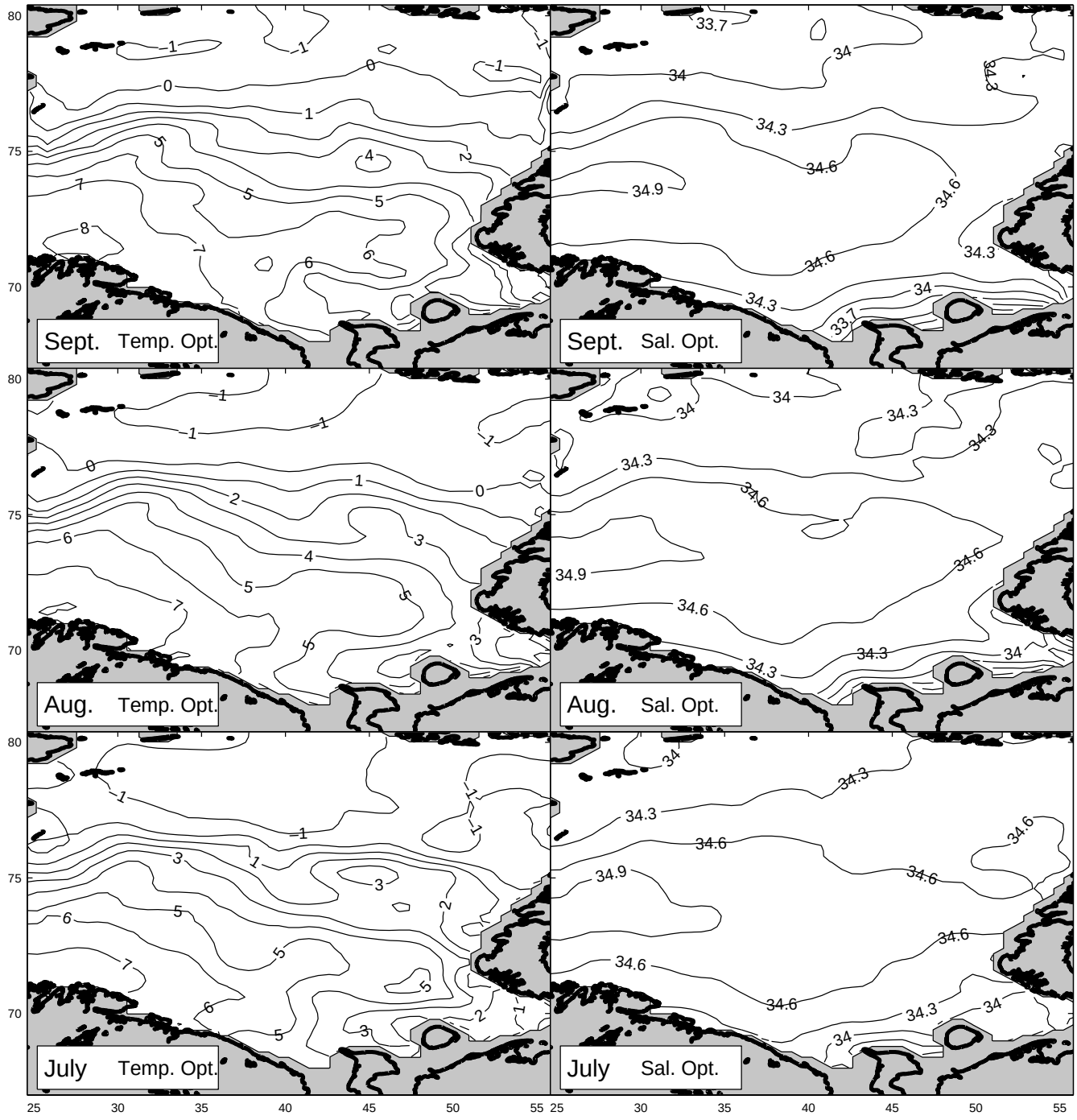

Fig. 5 Evolution of optimized temperature (left panels, °C) and salinity (right panels, psu) fields at 30-m depth.

in the description of local vertical mixing should be the more pronounced at this level. A sharp increase in $\varepsilon(z)$ (Fig. 6) at the 20–30 m level in August–September supports this speculation.

The salinity distribution in the BS is more uniform due to an intense inflow of relatively uniform high salinity water (34.6–34.9 psu) by the Norwegian Atlantic Current (Figs 1 and 2) and relatively small ($2–3 \times 10^{-7}$ kg m^{-2}) averaged surface salt fluxes in the summer season (Fig. 4). Strong changes in salinity occur in the northern and south-eastern regions of the BS, where ice melting (northern regions) and river runoff (south-eastern regions) strongly affect the salinity distribution.

The optimized velocity fields at 30 m and the evolution of summer SSH are presented in Fig. 7. In agreement with prior estimates of drifter velocity errors, the surface currents in Fig. 7 are rather close to the drifter velocity data in the western

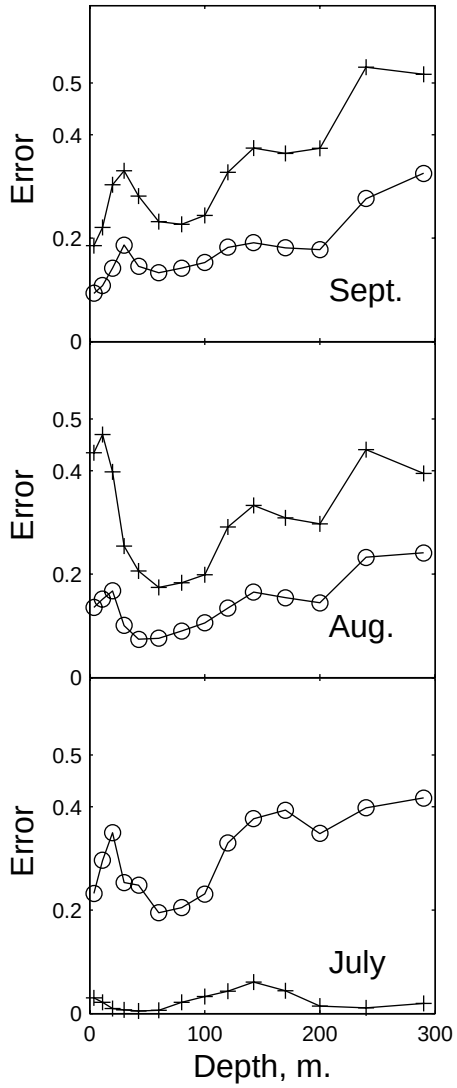

Fig. 6 Normalized differences between the climatological fields and the first guess solution (crosses), and climatological fields–optimized temperature field (circles) at different levels and months. The climatological temperature field is used as the initial condition for the first guess solution.

(25°E–30°E) part of the BS. In the region between 30°E and 40°E, the coincidence between drifter and model velocities gradually decreases due to larger drifter data errors.

In agreement with the schematics of the BS circulation (Fig. 1, Tantsiura (1959); Loeng et al., 1997), the Norwegian Atlantic Current flows into the BS, with velocities up to 20 cm s^{-1} through the western boundary and flows eastward forming two jets. One of these jets outflows through the Kara Gate, while another jet follows the 200-m isobath and splits into two unequal branches near NZ. The more intense of these branches deflects offshore forming a loop and then again follows the 200-m isobath. The second branch deflects onshore and flows along the coast of NZ. The onshore branch is weak in July but in August it gradually intensifies with velocities reaching 5 cm s^{-1} in September.

The northern branch of the Norwegian Atlantic Current follows the local topography (400-m depth isobath) and deflects northward. The major part of this branch recirculates through the western open boundary along the southern flank of Bear Island, while the remaining part flows north-eastward and forms the eastward current between Central and Great banks with an amplitude of 1–3 cm s^{-1}.

The currents north of 77°N are predominantly westward and south-westward with amplitudes of 2–7 cm s^{-1}. In the north-eastern region the westward currents are rather variable with time. The major branch of this current flows westward along the coast of FJL, while another branch turns southward and then flows out through the eastern open boundary, following the local topography. In the western BS, the south-westward currents are more stable and form a tongue of low salinity water (Figs 2 and 6, right panels) which enters the BS through the northern boundary.

The evolution of velocity and temperature fields at 200 m is shown in Fig. 8. Because of its barotropic origin, deep circulation resembles the circulation at the surface: the Norwegian Atlantic current flows into the BS, partly recirculates and forms two jets. The first jet follows the 200-m isobath, another jet, with velocities of about 2–5 cm s^{-1}, passes between the Central and Great banks. The locations of these jets correlate well with the locations of the tongues of warm water clearly seen in both climatological and optimized temperature fields at 200-m depth (Figs 3 and 9, right panels). Note that the amplitude of the optimized velocity decreases with depth in the north-eastern BS (Figs 7 and 8). Similar behaviour of the velocity field was observed by Loeng et al. (1993).

The optimized circulation pattern approximately agrees with the circulation scheme proposed by Tantsiura (1959), and adopted by other authors (e.g., Novitsky, 1961). However, there are two exceptions. In the reconstructed circulation one can notice the presence of an intense offshore branch of the NZ current and the current between the Central and Great banks (Figs 1, 7 and 8). These currents were recently described by Ozhigin et al. (2000) and Loeng and Satre (2001).

The variations of the onshore/offshore branches of the NZ current in July have a simple physical explanation based on the data used. According to Fig. 2, there is a temperature frontal zone at 73°N, 50°E near NZ in July, which prevents flow along NZ and amplifies the offshore current. This front disappears in September and the onshore branch of the NZ current becomes stronger.

The schematics of the circulation in the eastern BS were recently revised by Ozhigin et al. (2000), who found that the high salinity waters of the eastern BS are formed by significant transformation of Atlantic Water rather than having been carried by the Central current from the north-east (Tantsiura, 1959). High salinity waters form during cold winter periods along the NZ coast and at the Central Bank (Fig. 1) and then sink along the slope, inducing anticyclonic circulation in this region. Our results support this conclusion: Fig. 8 clearly

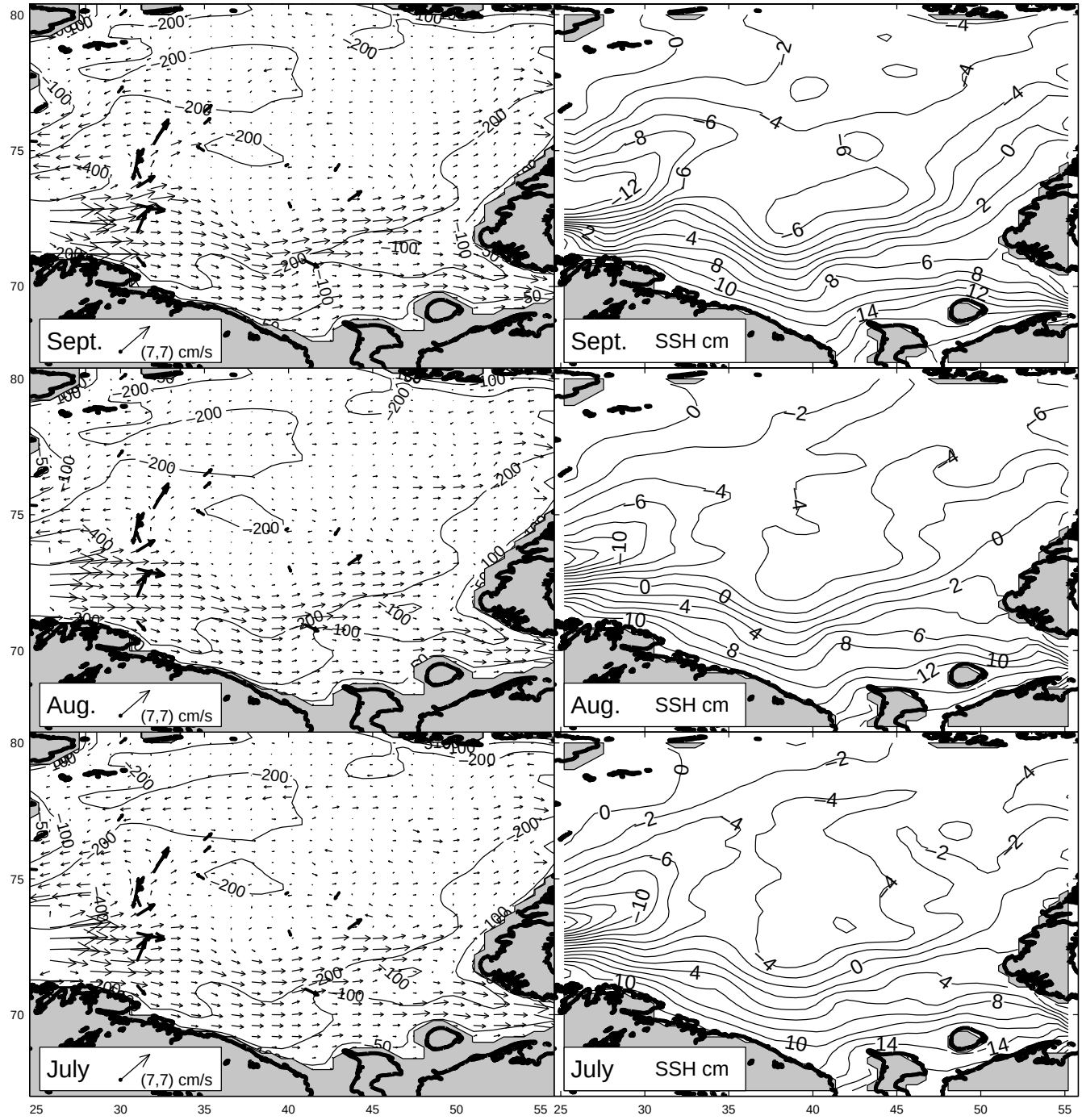

Fig. 7 Evolution of the optimized velocity at 30-m depth (left panels, cm s^{-1}) and SSH fields (right panels, cm). Thick arrows show the available historical velocity measurements averaged for different time periods (see Table B1 and Loeng and Saetre (2001)).

indicates predominantly north and north-eastward currents in the 42°–50°E and 71°–75°N region and weak south-westward and westward currents along the southern slope of the Central Bank.

The eastward current between the Central and Great banks was recently outlined by Loeng and Saetre (2001). The location of this current coincides with the location of the narrow tongue of warm water clearly seen in climatological temperature fields at 200-m depth between the Central and Great banks. Both direct velocity measurements (Fig. 7, thick arrows) and the results of Panteleev et al. (2004), based on the variational inversion of Acoustic Doppler Current Profiler (ADCP) and Conductivity-Temperature-Depth (CTD) measurements along 40°E longitude (Fig. 1), revealed an eastward

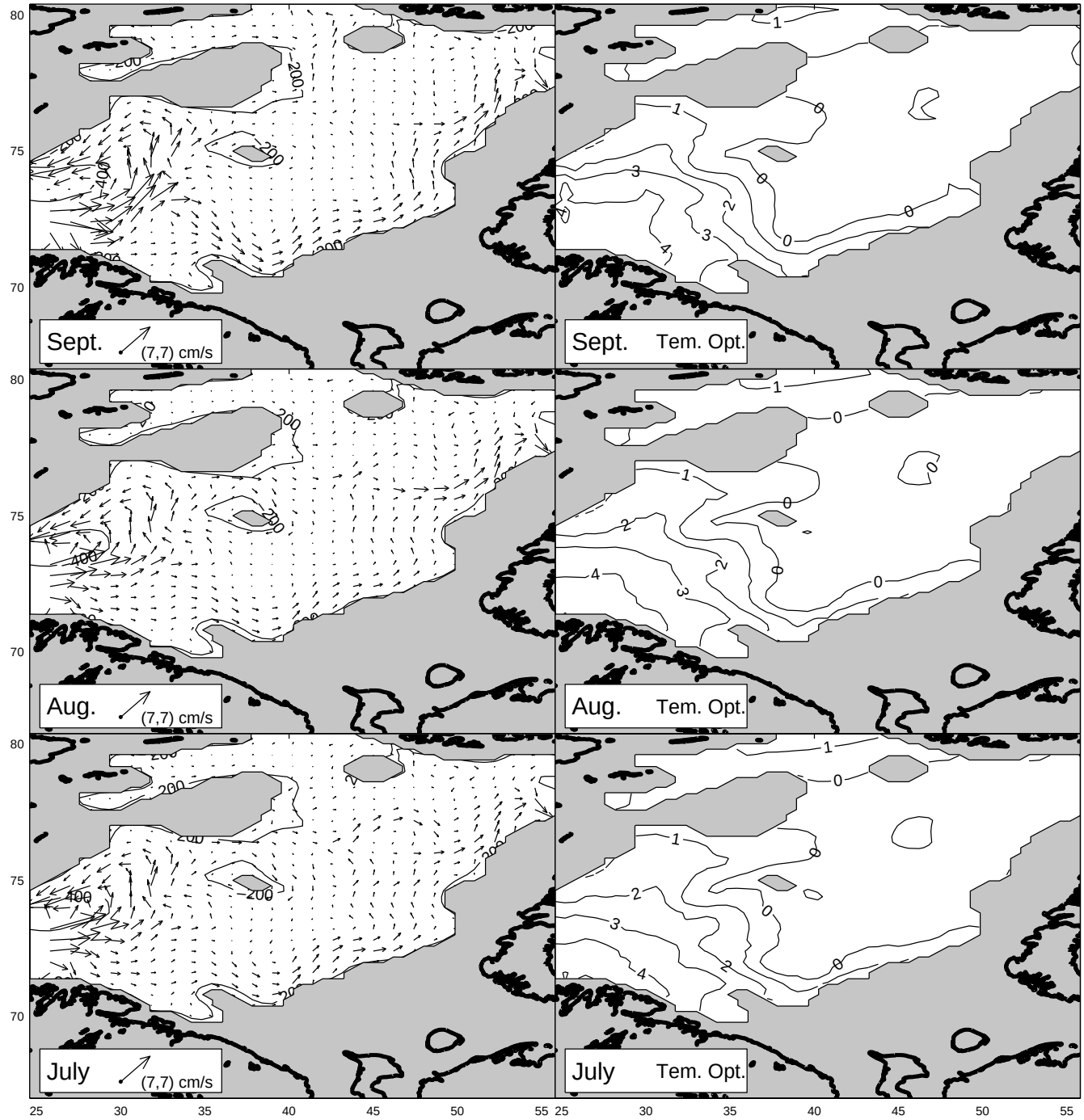

Fig. 8 Evolution of the optimized velocity (left panels, cm s^{-1}) and temperature (right panels, °C) fileds at 200-m depth.

current between 74°N and 76°N with a similar increase in velocity with depth. Therefore, the eastward current between the Central and Great banks in summer has both physical and observational confirmation. Finally, it is worth noting that a similar eastward current between the Central and Great banks and the north and north-east transport between the Central Bank and NZ was obtained in a diagnostic calculation of Yakovlev (1999).

The optimal circulation agrees with the drifter velocity data (Fig. 2). The data assimilation results in the reduction of the relative error

$$\varepsilon_u = \left(\sum_N \left(\mathbf{u} - \mathbf{u}^* \right)^2 / \sum_N \mathbf{u}^{*2} \right)^{\frac{1}{2}},$$

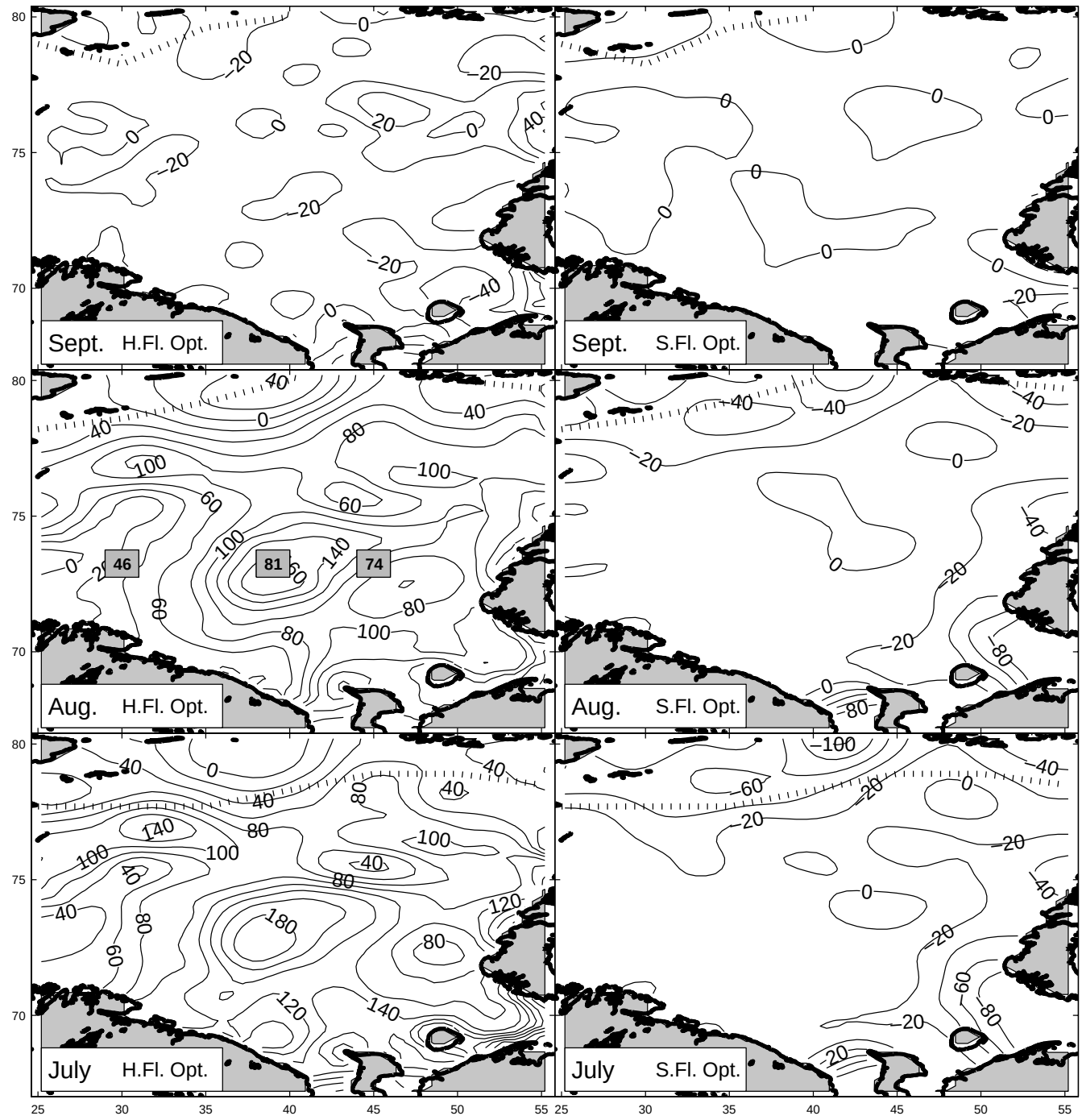

Fig. 9 Optimized surface heat (left panels, W m^{-2}) and salt fluxes (right panels, 10^{-7} kg m^{-2} s^{-1}). Dotted line indicates the location of the climatological ice edge for different months. The corresponding NCEP/NCAR surface heat fluxes are given in the boxes.

from 0.4–0.5 in the first guess solution to 0.25–0.35 in the optimized velocity field. In the region where the drifter data are assimilated, the amplitude of the velocities ranges between 5 and 15 cm s^{-1}. Therefore, the optimized velocities do not contradict the prior assumptions about the drifter velocity errors (Section 2b), while the velocities obtained in the first guess solution have larger errors.

The time-averaged direct velocity measurements (Loeng and Saetre, 2001) are shown in Fig. 7 by thick arrows. Since the velocity data were averaged over different time periods (from ten days up to one year), a straightforward comparison of the observations and modelled results is problematic. Therefore, we plotted all velocities for each month of the reconstructed circulation regardless of the actual time and duration of the observations. A

detailed description of these velocities can be found in Appendix B (Table B1). Regardless of how we treat such velocity observations statistically, we can see a reasonable correspondence between measured and optimized velocities. The least agreement between observed and optimized velocities can be seen in the region 74°–76°N and 31°–33°E. In part, this difference in velocities can be explained by an insufficient period of data averaging and strong variability of the current in this region. According to Table B1, velocities at the second mooring were averaged over only eight days, while the velocity measurements at the fourth mooring were averaged over one month and were half the magnitude. High variability of the local currents is clearly seen from the velocity measurements at 74°32′N and 30°58′E (lines 15–20 in Table B1): the observed velocities had almost opposite directions for different years. It is noteworthy that both direct velocity measurements in the central part of the BS and model results reveal cyclonic circulation in the region 72°–75°N, 38°–46°E. According to Ozhigin et al. (2000), generation of cold and saline water on the Central Bank and NZ shallows during the winter season (Midttun, 1985) and permanent export of this water into the basin between Central Bank and NZ creates cyclonic circulation in this part of the BS. The reconstructed summer circulation supports this conclusion.

Some circulation schemes (Tantsiura, 1959; Midttun and Loeng, 1986; Ozhigin et al., 2000) and results of numerical modelling of the BS circulation (Trofimov, 2000) suggest the presence of narrow currents along the Norwegian coastline and the southern part of NZ. These currents are the consequence of the local temperature/salinity fronts (see for example Fig. 2 in Ingvaldsen et al. (2002), and characterized by relatively warm and fresh water. Temperature and salinity climatology (ACSYS, 1999) do not capture these coastal currents (Fig. 2). Therefore, we do not exclude the possibility that utilization of a different dataset or consideration of a different season would modify the results of the reconstruction in this region. For example, Trofimov (2000) used the October temperature and salinity data derived from a database collected by the Polar Scientific Research Institute of Marine Fisheries and Oceanography, Murmansk, and obtained an intense north-eastward current along NZ. Notice that, in our results, the onshore branch of the NZ current and the Norwegian Coastal current showed strong intensification in September (Fig. 7) and we may assume that they intensified further in October.

The strong near-shore NZ current along the southern coast of NZ obtained by Yakovlev (1999), is probably a consequence of the total 0.015 Sv flow into the BS through the Kara Gate obtained in his results instead of the commonly accepted 0.6 Sv outflow from the BS into the Kara Sea. The reversed Kara Gate throughflow in the results of Yakovlev (1999) may prevent the eastward current in the southern part of the BS from exiting through the Kara Gate and redirect it backward along NZ.

b *Surface Fluxes*

Figure 9 shows the distribution of the optimized surface heat and salt fluxes in summer. The surface heat flux is roughly proportional to the difference between the atmospheric and sea surface temperature. Taking into account that spatial scales in the atmosphere are essentially larger than in the ocean, the "noisy" structure of the optimized heat fluxes seems to be realistic.

The spatial structure of the optimized surface salt fluxes (Fig. 9, right panels), is very uniform in the central and western parts of the BS with absolute values between $\pm 10.0 \times 10^{-7}$ kg m^{-2} s^{-1}. The surface salt flux depends on evaporation and precipitation. In the absence of strong temperature gradients between the sea surface and the atmosphere (the situation observed in the BS in summer), the evaporation and precipitation should have a meteorological spatial scale. So, the spatial structure of salt fluxes obtained in the western and central parts is physically reasonable.

The optimized surface salt fluxes in the northern and eastern regions of the BS are negative and range from -20×10^{-7} kg m^{-2} s^{-1} to -100×10^{-7} kg m^{-2} s^{-1}. During July and August, the strong negative salt fluxes in the northern region (78°–80°N) of the BS correlate with weak positive (0–40 W m^{-2}) and negative (–30 to 0 W m^{-2}) surface heat fluxes. Taking into account the small influence of the advective processes on the evolution of the ice cover in the BS (Makshtas and Ivanov, 1990), we can explain this correlation by the ice melting in July and August, and the gradual retreat of the ice edge shown in Fig. 9 by the dotted line. The ice edge locations observed in August and September are close to each other indicating an equilibrium of the ice melt and growth processes. The optimized solution reveals the corresponding decrease in amplitude of the heat and salt surface fluxes in the northern regions of the BS in September (Fig. 9).

The influence of negative surface salt fluxes with an amplitude of $50–100 \times 10^{-7}$ kg m^{-2} s^{-1} during July and August is approximately equivalent to the ice melting at an average rate of 0.25–0.50 m mo^{-1}. Nikolaev et al. (1984) reported that typical ice thickness in the marginal zones is 0.8–1.5 m, with ice concentration gradually increasing from 0 up to 100% within a distance of about 100 km from the ice edge. Under the assumption that in August and September ice is imported into the BS and then melts in the vicinity of the ice edge, the reconstructed salt flux magnitude gives a typical mean ice thickness estimate of 0.5–1.0 m, which is in agreement with the independent estimates of Nikolaev et al. (1984).

According to Fig. 9, the maximum positive heat fluxes are located in the central (73°N, 39°E) part of the BS in July and August. We used the results of the National Centers for Environment Prediction/National Center for Atmospheric Research (NCEP/NCAR) reanalysis (http://www.cdc.noaa.gov/cdc/reanalysis/index.html) and estimated the mean surface heat flux for the following regions (73°N, 30°E), (73°N, 39°E), (73°N, 45°E) during August, which were found to be 46, 81 and 74 W m^{-2} respectively. These numbers are also plotted in Fig. 9. As can be seen, the August NCEP/NCAR surface heat fluxes reveal a maximum at 73°N, 39°E and a significant decrease in the surface heat fluxes in the western part of the BS. We speculate that the pattern of surface heat fluxes is associated with local surface temperature distribution (Fig. 2, left panels), which

reveals the spot of relatively cold water in July–August at 73°N, 39°E.

A simplified description of vertical mixing may cause significant errors in temperature and salinity evolution in shallow regions. Because of that, the negative salt fluxes in the south-eastern part of the BS may indicate an artificial model response. At the same time, our model utilizes boundary conditions with zero heat and salt fluxes along the lateral boundaries, and does not take into account some important processes such as river discharge (e.g., the Pechora river) or summer glaciers melting on NZ. Therefore, the negative salt fluxes can also be treated as compensation for zero lateral boundary fresh water fluxes. Note that the magnitude of negative salt fluxes along NZ and in the northern BS decreases in September when the drop in the air temperature should decrease the fresh water discharge.

In order to analyse the obtained heat fluxes in the central part of the BS, we grouped the available estimates in Table 2. It can be seen that the optimized heat fluxes are in a good agreement with the observations of Makshtas and Ivanov (1997), are in slightly poorer agreement with the NCEP/NCAR reanalysis results and are approximately 30–50 W m^{-2} higher than the heat fluxes of da Silva et al. (1995). Since da Silva et al. (1994) and the NCEP/NCAR climatological fields are over smoothed in the BS and in the Arctic, we believe that the reconstructed heat fluxes are more realistic than da Silva and NCEP/NCAR climatologies and reflect the local features of the BS circulation better.

TABLE 2 Estimates of the surface heat flux (W m^{-2}) for the central part of the BS taken from: (1) da Silva (1995), climatology; (2) NCEP/NCAR reanalysis (http://www.cdc.noaa.gov/cdc/reanalysis/index.html); (3) Makshtas and Ivanov (1997); (4) Panteleev et al. (2003); and (5) estimated in this paper.

Month,	(1)	(2)	(3)	(4)	(5)
July	100	155	140	–	80 – 180
Aug.	30	75	100	–	60 – 160
Sept.	–50	–25	–	10	–20 – +10
Oct.	–140	–160	–80	–	–

c *Error Estimates*

The standard posterior error analysis through the inversion of the Hessian matrix associated with the cost function, Eq. (1), (Thacker, 1989) is computationally prohibitive in our study because of the large dimension (250,000 elements) of the control vector. Therefore, we conducted the posterior error analysis based on a sample variance estimate for an ensemble of data assimilation results.

Since the circulation in the BS is essentially barotropic, it is reasonable to assume that the uncertainties in the drifter velocity data and the errors in transport estimates are a major contribution to the uncertainties of the assimilated solution. If so, the error covariance of the optimized velocities and/or SSH can be estimated as the covariance of the ensemble of optimal solutions generated by adding random noise (with the amplitude of the corresponding data error, see Sections 2b and 2c) to drifter velocities and transport estimates. Drifter data provide information on the Norwegian Atlantic current and can be treated as one datum. Consequently we disturb only six parameters (five estimates of the transport and drifter velocity amplitude) in order to determine the major part of the uncertainties of the velocity and SSH fields in the BS.

Following the hypothesis outlined, we conducted ten constrained minimizations of the cost function, Eq. (1), with the perturbed "barotropic" data (drifter velocities and transport estimates) and computed the field of normalized standard deviation for the ensemble of optimal velocities and standard deviation estimate for the ensemble of optimal SSH. Because of limited ensemble dimension (ten elements), the derived fields were smoothed with a 130-km cut-off spatial filter and the final results are presented in Fig. 10.

The analysis of Figs 7 and 10 demonstrates that the obtained climatological summer circulation is statistically reliable in the major part of the BS. The regions with strong relative variability in the ensemble are located in the northern part of the BS, near NZ and in Bear Island Trough. Note that the error analysis reveals a relatively high level of variability at 75°N, 31°S, that is in the location where long-term velocity observations also show strong variability in the currents (see Fig. 7 and Table B1).

According to Fig. 10, the reconstructed current between the Great and Central banks and cyclonic circulation between Central Bank and NZ are relatively reliable, while some of the commonly accepted features are not. For example, the circulation scheme proposed by Tantsiura (1959), indicates the presence of a continuous westward current in the northern part of the BS (Fig. 1). Our results (Fig. 7) show a similar current in July, but the error analysis shows that the statistical reliability of this current is very weak (Fig. 10, left panels). Note that in August and September the reconstruction of the circulation in the northern BS is more reliable than in July, but the westward current entering through the eastern boundary of the region does not continue to flow westward and retroflects eastward near 79°N, 50°E.

One of the potential problems in the variational approach is the sensitivity of the optimized solution with respect to the choice of the first guess solution. A set of numerical experiments started from different first guess solutions has revealed very small changes in the optimized SSH, velocity, temperature, salinity, wind stress fields, and moderate variability in the optimized surface heat flux at the beginning and end of the data assimilation period. Sensitivity of the surface heat and salt fluxes with respect to the first guess solution may have several explanations. Firstly, the absence of surface heat flux data in the cost function, Eq. (1) allows these fields to vary within a broader range than other model variables, which are constrained by data. Secondly, in the middle of the assimilated period (August), the optimized model solution is constrained by a larger amount of temperature and salinity data than at the end and/or beginning of the period.

Based on the error analysis and the sensitivity study of the data assimilation results we may conclude that the problem of the

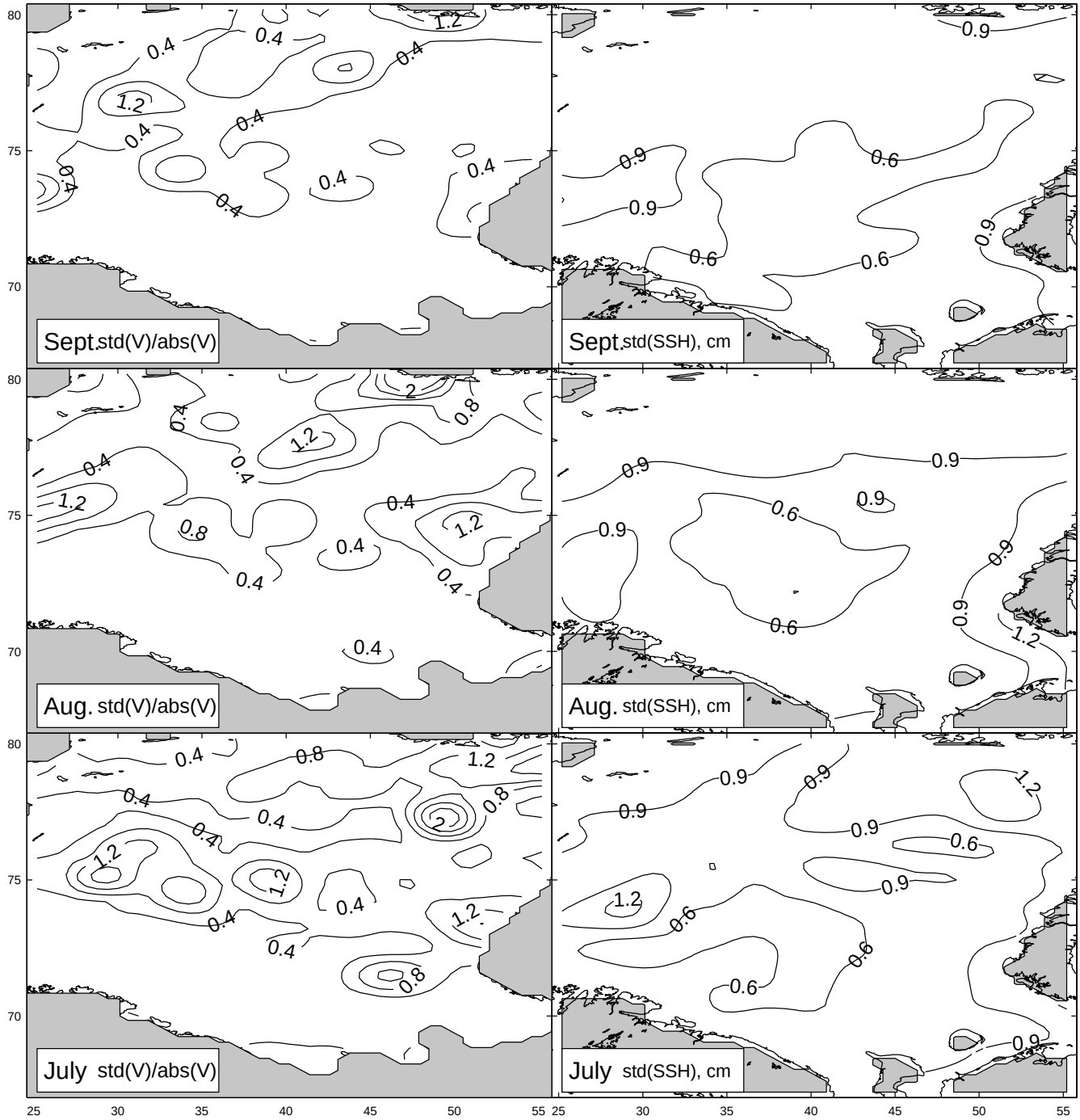

Fig. 10 Distribution of the normalized standard deviation ($\sigma_{\mathbf{u}}$/abs($\overline{\mathbf{u}}$)) for the ensemble of optimal velocities (left panels) and standard deviation for the ensemble of the optimal SSH (right panels, cm).

reconstruction of the summer BS circulation from climatological data is well posed. Well-posedness of the problem is conditioned by the proper choice of the non-eddy resolving parameters and grid resolution of the model, by introduction of smoothness terms into the cost function, Eq. (1), and reduction of the control vector dimension. The latter was achieved through the linear interpolation in time of the boundary conditions of the model.

From the dynamical point of view, the well-posedness of the data assimilation problem can be illustrated as follows. Within the frames of the non-eddy resolving nearly geostrophic dynamics, the fields of temperature, salinity and wind stresses determine the vertical shear of the velocity in the BS. Given the low frequency of variability of these fields in the model, these fields are well constrained by hydrographic and wind stress

data. To recover the absolute or reference velocity in the BS, the model imposes additional volume, heat, and salt mass balance constraints on the circulation. Additional data sources such as surface velocities and transport estimates, combined with the bogus data enforcing smoothness of the optimal fields, make the reconstructed absolute velocity more reliable.

5 Summary

We present a quantitative estimate of summer climatological circulation in the BS derived from hydrographic and velocity observations. The circulation is obtained through the variational optimization of initial and boundary conditions of a non-eddy resolving ocean model. The optimized circulation is dynamically balanced within the framework of the model and consistent with the evolution of temperature and salinity fields documented in the BarKode hydrophysical atlas (ACSYS, 1999).

The climatological circulation is characterized by an intense (3.2 Sv) Norwegian Atlantic Current, with average velocities reaching 10–15 cm s^{-1}. Approximately 1.5 Sv of this inflow recirculates along the northern flank of Bear Island Trough, while the major branch of the current crosses the BS and flows out through the FJL–NZ and Kara Gate straits with transports of 1.1 Sv and 0.7 Sv, respectively. The optimized transport between 73°N and the Norway coast gradually increases from 2.9 Sv in July, to 3.1 Sv in August and 3.6 Sv in September. These values are in good agreement with the independent estimate of the mean summer inflow of 3.1 Sv obtained by Ingvaldsen et al. (2002).

The circulation is in agreement, with a general scheme proposed by Tantsiura (1959) and adopted by other authors (e.g., Novitsky, 1961; Loeng et al., 1997). In addition, the data assimilation is able to reconstruct the details, which had been missed in the general circulation scheme. The optimized solution reveals an eastward current between Great and Central banks and cyclonic circulation in the region between Central Bank and NZ. These circulation features have recently been confirmed in a number of publications (Ozhigin et al., 2000; Loeng and Saetre, 2001).

The reconstructed surface heat and salt fluxes can be treated as independent estimates of the surface heat and salt fluxes in the BS region. Good agreement with available climatological estimates (da Silva et al., 1994; Kalnay et al., 1996) and actual measurements (Makshtas and Ivanov, 1997) allows us to suggest that similar estimates can be obtained for other parts of the Arctic Ocean. Flux estimates derived from hydrographic data by an inverse method could be very useful in the regions covered by ice, providing an alternative estimate for poorly known fluxes at the sea-ice boundary.

The error analysis and the study of sensitivity with respect to the choice of the first guess solution demonstrate that our results are statistically reliable. The highest reliability is achieved in the middle of the assimilation period, while the results at the beginning and the end of the assimilation period can be influenced by the uncertainties in the first guess solution.

Finally, we would like to note that the data assimilation approach has a strong advantage compared with the traditional estimates of the ocean state obtained through the geostrophic calculations and numerical modelling. The main advantage of the circulation obtained from data assimilation is that it agrees closely with the existing data and that all circulation fields (temperature, salinity, velocity, surface heat, salt and momentum fluxes) are dynamically balanced and provide the information on the evolution of the currents. The geostrophic calculations can only use one type of data (temperature/salinity) and may only reproduce the circulation averaged over the data period. The application of a high resolution OGCM allows us to obtain the non-stationary climatological currents and partially take into account different types of data, but these results are usually obtained by using the nudging (or restoring) technique (for example Maslowski et al. (2004)), which strongly violates the conservation of heat and salt in the model (Awaji et al., 2003). The variational technique has proved to be extremely flexible and robust (Stammer et al., 2002). The 4D-var data assimilation algorithm used has demonstrated a very high level of efficiency and controllability. This is the result of semi-implicit non-linear model formulation (Nechaev and Panteleev, 2000), which was developed specifically for the solution of the 4D-var problem. The potential drawback of the data assimilation model used is the simplified parametrization of the vertical mixing. In future we are planning to incorporate the K-profile parametrization (KPP) vertical mixing scheme (Large et al., 1994) and its adjoint into the inverse model.

Acknowledgments

This study was funded by the Frontier Research System for Global Change, through the Japan Agency for Marine-Earth Science and Technology (JAMSTEC) Japan, and the sponsorship of the International Arctic Research Center (IARC). The development of the data assimilation system used in this study was also supported by an Office of Naval Research (ONR) grant N00014-00-1-0201 and a National Science Foundation (NSF) grant OCE-01-18200. We thank A. Zuev and A. Trofimov for helpful discussions and valuable assistance.

Appendix A

A standard way to parametrize convective adjustment in hydrostatic systems is to represent this process in the form of non-linear diffusion:

$$\hat{\Pi}\rho = \mu\partial_z\theta(\rho_z)\partial_z\rho,$$

where

$$\theta(x) = \begin{cases} 0, & x \le 0 \\ 1, & x > 0 \end{cases} \qquad \text{(A1)}$$

and μ is a sufficiently large constant, so that the convective relaxation timescale is much shorter than the timescales of the fastest processes resolved by the system. In the present study we use a standard approximation of $\hat{\Pi}$ which is usually called

the finite-difference convective adjustment scheme. The operator $\hat{\Pi}$ is represented in the form

$$\hat{\Pi} = \prod_{s=1}^{N(\rho)} \hat{\Pi}_{k(s)}$$

where $\hat{\Pi}_{k(s)}$ is the "elementary" mixing operator, performing a mass-conserving average between the layers ρ_k and ρ_{k+1}:

$$\hat{\Pi}_k = \begin{Vmatrix} 1 & 0 \\ 0 & 1 \end{Vmatrix} + \frac{1}{2}\theta(\Delta\rho_k) \begin{Vmatrix} -1 & 1 \\ 1 & -1 \end{Vmatrix};$$

and $N(\rho)$ is the total number of elementary mixing events necessary to project a given profile $\{\rho_k\}$, $k = 1,..., K$ onto the one with $\Delta\rho_k \equiv \rho_k - \rho_{k+1} \le 0$ (for simplicity we assume homogeneity of the vertical grid $\delta_{z_1} = \delta_{z_2} = ... = \delta_{z_K}$). The tangent linear operator to $\hat{\Pi}_k$ is

$$\hat{\Pi}'_k = \hat{\Pi}_k + \frac{1}{2}\Delta\rho_k\delta(\Delta\rho_k) \begin{Vmatrix} -1 & 1 \\ 1 & -1 \end{Vmatrix} = \hat{\Pi}_k.$$

Therefore the adjoint finite difference convective adjustment can be represented in the form

$$\hat{\Pi}^T = \prod_{N(\rho)}^{s=1} \hat{\Pi}^T_{k(s)}.$$

In practice we have to store space-time coordinates of all the elementary convective events during the "forward" run of the model and then apply their transposes in the reverse order when running the adjoint code.

Appendix B

From the early 1970s until 1996 the current measurements in the BS have been carried out at more than 70 locations by different Norwegian institutions. Unfortunately, most of the results were published in data reports with limited accessibility. Loeng and Saetre (2001) provide the analysis of these velocity measurements in the BS and present the time-averaged velocities at each current meter. In Table B1 we reproduce the time-averaged velocity values (Loeng and Saetre, 2001) obtained at 25 moorings located inside the model domain and shown in Fig. 7. Note that the time period for averaging of velocity data varies for different current meters from 8 days to 400 days. Also, not all of the data correspond to the summer season. This complicates the quantitative comparison of the current meter data with data assimilation results.

TABLE B1. Summary of the time-averaged mooring velocities described by Loeng and Saetre (2001). Current meter locations are shown in Fig. 7.

N	Position (°N, °E)	Depth (m)	start/stop days	u cm s^{-1}	v cm s^{-1}
1	75°00′ 34°57′	50	18.09.88–28.10.88	–1.52	1.14
2	75°15′ 31°59′	45	11.07.79–19.07.79	3.40	6.68
3	74°00′ 31°11′	50	25.06.81–07.07.81	–1.03	2.82
4	75°29′ 32°10′	25	05.07.81–08.08.81	2.68	3.98
5	73°05′ 40°01′	25	25.08.89–21.10.89	0.47	–1.21
6	74°30′ 39°58′	20	26.08.89–10.10.89	–0.54	–0.45
7	74°30′ 43°01′	25	26.08.89–24.10.89	–1.00	–1.73
8	76°00′ 34°60′	60	13.09.92–30.09.93	1.32	1.37
9	76°26′ 34°59′	60	13.09.92–30.09.93	1.70	1.70
10	80°00′ 30°00′	75	30.07.80–25.08.81	1.70	1.70
11	71°04′ 31°00′	30	19.09.89–18.10.89	1.81	–2.40
12	72°30′ 31°00′	100	19.09.89–22.11.89	3.45	3.33
13	73°00′ 31°00′	50	18.09.89–22.11.89	6.40	–1.60
14	73°40′ 31°01′	100	18.09.89–22.11.89	3.96	2.88
15	74°32′ 30°58′	50	01.07.85–01.08.85	1.23	3.38
16	74°32′ 30°58′	50	01.08.85–01.09.85	1.41	0.75
17	74°32′ 30°58′	50	01.09.85–01.10.85	–0.84	–4.32
18	74°32′ 30°58′	50	01.07.86–01.08.86	1.57	3.89
19	74°32′ 30°58′	50	01.08.86–01.09.86	0.38	3.58
20	74°32′ 30°58′	50	01.09.86–01.10.86	1.23	1.32
21	75°20′ 25°01′	25	12.11.87–03.06.88	–2.69	0.24
22	70°57′ 41°00′	75	14.09.94–15.09.95	3.03	–1.75
23	77°09′ 29°52′	85	03.10.93–10.09.94	1.01	1.49
24	72°00′ 31°00′	50	01.09.89–30.09.89	2.09	5.73
25	73°10′ 43°34′	50	07.08–03.09	2.99	2.51

References

AAGAARD, K.; J.H. SWIFT and E.C. CARMACK. 1985. Thermohaline circulation in the Arctic Mediterranean seas. *J. Geophys. Res.* **90**: 4833–4846.

[ACSYS] ARCTIC CLIMATE SYSTEM STUDY. 1999. Barents and Kara Seas Oceanographic Data Base (BarKode) [CD-ROM], Tromso, Norway. Available from (http://acsys.npolar.no./adis/datasets/barkode/barkode.php). ACSYS/CLIC International Project Office.

AWAJI, T.; S. MASUDA, Y. ISHIKAWA, N. SUGIURA, T. TOYODA and T. NAKAMURAA. 2003. State estimation of the North Pacific Ocean by a four-dimensional variational data assimilation experiment. *J. Oceanogr.* **59**: 931–943.

BLINDHEIN, J. 1989. Cascading of Barents Sea bottom water into the Norwegian Sea. *Rapp. P.-v Reun. Cons. Int. Explor. Mer.* **188**: 161–189.

DA SILVA, A.; C.C. YOUNG and S. LEVITUS. 1994. Atlas of surface marine data, Volume I: Algorithms and procedures. NOAA Atlas NESDIS 6, U.S. Department of Commerce, Washington, D.C.

DENISOV, V.V; A.N. ZUYEV, I.A. LEBEDEV and V.N. SHIROKOLOBOV. 1987. On the research of hydrological conditions of the Barents Sea based on interdepartmental multidisciplinary expeditions. In*: Multidisciplinary oceanographic research in the Barents and White Seas*. Appatity. Izdat. Kola filial of AN SSSR, pp. 9–13.

FUREVIK T. 2001. Annual and interannual variability of Atlantic Water temperature in the Norwegian and Barents Seas: 1980–1996. *Deep-Sea Res.* **48**: 383–403.

GILBERT, J.C. and C. LEMARECHAL. 1989. Some numerical experiments with variable storage quasi-Newton algorithms. *Math. Prog.* **45**: 407–455.

GOLUBEV, V.A.; A.N. ZUYEV and I.A. LEBEDEV. 1992. Methods of processing and objective analysis of oceanographic data. Trudy AANII *In:* Proc. Arctic Antarctic Institute, Vol. 426, pp. 7–19.

GROTOV, A.S.; D.A. NECHAEV, G.G. PANTELEEV and M.I. YAREMCHUK. 1998. Circulation in Bellingshausen and Amundsen Seas. *J. Geophys. Res.* **103**: 13011–13023.

HARMS, I.H. 1997. Water mass transformation in the Barents Sea. *J. Mar. Sci.* **54**: 53–64.

HAUGAN, P. 1999. On the transports of mass, heat and carbon in the Arctic Mediterranean. PhD Thesis, University of Bergen, Norway, 166 pp.

HELLAND-HANSEN, B. 1934. Oceanographic observations in the northernmost part of the North Sea and southernmost part of the Norwegian Sea. *In*: *James Johnstone Memorial Volume*, University of Liverpool Press, pp. 257–274.

INGVALDSEN, R.; H. LOENG and L. ASPLIN. 2002. Variability in the Atlantic inflow to the Barents Sea based on a one-year time series from moored current meters. *Cont. Shelf Res.* **22**: 505–519.

——; L. ASPLIN and H. LOENG. 2004. Velocity field of the western entrance to the Barents Sea. *J. Geophys. Res.* **109**: c03021, doi:10.1029/203JC001811.

JONES, E.P.; L.G. ANDERSON and J.H. SWIFT. 1998. Distribution of Atlantic and Pacific waters in the upper Arctic Ocean: implications for circulation. *Geophys. Res. Lett.* **25**: 765–768.

KALNAY, E.; M. KANAMITSU, R. KISTLER, W. COLLINS, D. DEAVEN, L. GANDIN, M. IREDELL, S. SAHA, G. WHITE, J. WOOLLEN, Y. ZHU, A. LEETMAA, B. REYNOLDS, M. CHELLIAH, W. EBISUZAKI, W. HIGGINS, J. JANOWIAK, K. C. MO, C. ROPELEWSKI and J. WANG. 1996. The NCEP/NCAR 40-year reanalysis project. *Bull. Am. Meteorol. Soc.* **77**: 437–471.

LARGE, W.G.; J. C. MCWILLIAMS AND S.C. DONEY. 1994. Oceanic vertical mixing: a review and a model with a non-local boundary layer parameterization. *Rev. Geophys.* **32**: 363–403.

LEDIMET, F.X. and O. TALAGRAND. 1986. Variational algorithms for analysis and assimilation of meteorological observations: theoretical aspects. *Tellus*, **38A**: 97–100.

LOENG H.; V. OZHIGIN, R. ADLANSVIK and H. SAGEN. 1993. Current measurements in the northeastern Barents Sea. ICES C.M, C:22 pp.

——; —— and ——. 1997. Water fluxes through the Barents Sea, *ICES J. Mar. Sci.* **54**: 310–317.

—— and R. SAETRE. 2001. Features of the Barents Sea circulation. Project report, HAVFORSKNINGSINSTITUTTET, ISSN 0071-5638. pp. 1–40.

LOYNING, T.B. 2000. Hydrography in the north-western Barents Sea July–August 1996. *Polar Res.* **20**(1): 1–12.

MORK, K.A. and J. BLINDHEIM. 2001. Variations in the Atlantic inflow to the Nordic Seas, 1955–1996. *Deep-Sea Res.* **47**: 1035–1057.

MADEC, G.; P. DELECLUSE, M. IMBARD and C. LEVY. 1999. OPA8.1 Ocean General Circulation Model. Reference Manual, Note du Pole modelisation, Institute Pierre-Simon Laplace (IPSL), France, 91 pp.

MAKSHTAS, A.P. and B.V. IVANOV. 1990. Spatial and temporal variability of the ice distribution in the regions of its seasonal migration. *In*: Proc. Arctic Antarctic Research Institute. Numerical modeling of the ice coverage: now- and forecast. Hidrometeoizdat, Leningrad, pp. 71–80, (in Russian).

—— and ——. 1997. Features of sea/air energy exchange processes in the zone of seasonal migration of drifting sea ice. Natural conditions of the Kara and Barents seas. *In*: Proc. Russian-Norwegian Workshop-95, 28 Feb. – 2 March 1995, Norsk Polarinstitutt, Oslo, pp. 152–159.

MARCHUK, G.I. 1974. Basic and adjoint equations of the ocean and atmosphere dynamic. *Meteorologija and gidrologija* **6**: 17–34.

MASLOWSKI, W.; D. MARBLE, W. WALCZOWSKI, U. SCHAUER, J. CLEMENT and A. SEMTNER. 2004. On climatological mass, heat, and salt transports through the Barents Sea and Fram Strait from a pan-Arctic coupled ice-ocean model simulation. *J. Geophys. Res.* **109**(C3): C03032, 10.1029/2001JC001039.

MATISHOV, G.; A. ZUEV, V. GOLUBEV, N. ADROV, V. SLOBODIN, S. LEVITUS and I. SMOLYR. 1998. Climate atlas of the Barents Sea 1998: temperature, salinity, oxygen. 35 pp. (Available on CD-ROM.)

MIDTTUN, L. 1985. Formation of dense bottom water in the Barents Sea. *Deep-Sea Res.* **32**: 1233–1241.

—— and H. LOENG. 1986. Climate variations in the Barents Sea. *In*: Proc. Third Soviet-Norwegian Symposium, The effect of oceanographic conditions on distribution and population dynamics of commercial fish stocks in the Barents Sea. H. Loeng (Ed.), Murmansk, pp. 13–28.

NECHAEV, D. and G. PANTELEEV. 2000. Baroclinic model of the Korea/Tsushima Strait. EOS, Transaction, AGU, Vol. 81, No. 48.

——; M. YAREMCHUK and M. IKEDA. 2004. Decadal variability of circulation in the Arctic Ocean retrieved from climatological data by a variational method. *J. Geophys. Res.* **109**: C04006, doi: 10.1029/2002JC001740.

NIKOLAEV, Y.V.; A.P. MAKSHTAS and B.V. IVANOV. 1984. Physical processes in the marginal zones. *Meteorol. Hydrol.* **11**: 73–80.

NOVITSKY, V.P. 1961. Permanent currents of the northern Barents Sea. *Trudy Gosudarsvtennogo Okeanograficheskogo Instituta*, **64**: 1–32. (Translated by U.S.N.O. 1967.)

OZHIGIN, V.K.; A.G. TROFIMOV and V.A. IVSHIN. 2000. The eastern basin water and currents in the Barents Sea. *ICEAS Annual science Conference*, L:14.

PACANOWSKI R. C. and G. H. PHILANDER. 1981. Parameterization of vertical mixing in numerical models of tropical oceans. *J. Phys. Oceanogr.* **11**: 1443–1451.

PANTELEEV, G.; M. IKEDA, A. GROTOV, D. NECHAEV and M. YAREMCHUK. 2004. Mass, heat and salt balances in the eastern Barents Sea obtained by inversion of hydrographic section data. *J. Oceanogr.* **60**: 613–623.

PENENKO, V.V. 1981. *Methods of numerical simulation of atmospheric processes.* Hydrometeoizdat, 347 pp.

PFIRMAN, S.L.; D. BAUCH and T. GAMMELSROD. 1994. The northern Barents Sea: Water mass distribution and modifications. *In: The Polar Oceans and Their Role in shaping the Global Environments*. *Geophys. Monogr. Ser*. Vol. 85, O.M. Johannessen, R.D. Muech, and J.E. Overland (Eds), AGU, Washington. D.C., pp.74–94.

POTANIN, V.A. and S.V. KOROTKOV. 1988. Seasonal variability of the main currents in the southern Barents Sea and water exchange with the adjacent areas. *In*: Proc. Geological and Geographical Problems of natural resources exploitation in the Northern Seas. Murmansk, pp. 81–90, (in Russian).

POULAIN P.-M.; A. WARN-VARNAS and P.P. NIILER. 1996. Near-surface circulation of the Nordic seas as measured by Lagrangian drifters. *J. Geophys. Res.* **101**: 18237–18258.

SCHAUER, U.; H. LOENG, B. RUDELS, V.K. OZHIGIN and W. DIECK. 2002. Atlantic water flow through the Barents and Kara Seas. *Deep-sea Res. (I)* **49**: 2281–2298.

SCHERBININ, A. 2001. Measurements in the Kara Strait. In: *Experience of system oceanologic studies in the Arctic*. Scientific World, Moscow. pp.128–133.

STAMMER, D.; C. WUNSCH, R. GIERING, C. ECKERT, P. HEIMBACH, J. MAROTZKE, A. ADCROFT, C.N. HILL and J. MARSHAL. 2002. Global circulation during 1992–1997, estimated from ocean observations and a general circulation model. *J. Geophys. Res.* **107**(C9): 3118, doi:10.1029/2001JC000888.

TANTSIURA, A.I. 1959. On the currents of the Barents Sea. Transactions of the Polar Scientific Research Institute of Marine Fisheries and Oceanography, - N.M. Knipovic (PINRO), 11, pp. 35–53, (in Russian, translated to English by the Norwegian Polar Research Institute, Oslo, 1983).

THACKER, W. C. 1989. The role of the Hessian matrix in fitting models to measurements. *J. Geophys. Res.* **94**: 6177–6196.

TIMOFEEV, V.T. 1963. Water interaction between the Arctic, Atlantic and Pacific Oceans. *Oceanology*, **3**: 569–578, (in Russian).

—— and R. LONG. 1988. Fitting dynamics to data. *J. Geophys. Res.* **93**: 10655–10665.

TROFIMOV, A.G. 2000. Numerical modelling of the Barents Sea circulation. Ph. D. Thesis, Izdatel'stvo Pinro, Murmansk, 42 pp, (in Russian).

URALOV, N.S. 1960. On the advective component of the heat balance in the southern Barents Sea. *Trudy Gosudarstvennogo Oceanograficheskogo Instituta*, **55**: 3–20 (in Russian).

WUNSCH, C. 1996. The ocean circulation inverse problem. Cambridge University Press, Cambridge. 442 pp.

YAKOVLEV, N. 1999. Reconstruction of monthly mean circulation of the Barents Sea and analysis of circulation sensitivity to water exchange at open boundaries. *Izvestiya Akademii nauk, Fizika Atmospheri i Okeana* **35**: 846–857.